Microscopic Dynamics in the Strain Hardening Regime of Glassy Polymers

Jérôme Hem, Caroline Crauste-Thibierge, Thomas Merlette, Florence Clément, Didier Long, Sergio Ciliberto

▶ **To cite this version:**

Jérôme Hem, Caroline Crauste-Thibierge, Thomas Merlette, Florence Clément, Didier Long, et al.. Microscopic Dynamics in the Strain Hardening Regime of Glassy Polymers. Macromolecules, 2022, 55 (20), 10.1021/acs.macromol.2c00802 . hal-03819002v2

HAL Id: hal-03819002
https://hal.science/hal-03819002v2

Submitted on 14 Nov 2022

HAL is a multi-disciplinary open access archive for the deposit and dissemination of scientific research documents, whether they are published or not. The documents may come from teaching and research institutions in France or abroad, or from public or private research centers.

L'archive ouverte pluridisciplinaire **HAL**, est destinée au dépôt et à la diffusion de documents scientifiques de niveau recherche, publiés ou non, émanant des établissements d'enseignement et de recherche français ou étrangers, des laboratoires publics ou privés.

Microscopic dynamics in the strain-hardening regime of glassy polymers

J. Hem[1], C. Crauste-Thibierge[1], T. Merlette[2], F. Clément[2], D.R. Long[2,3], S. Ciliberto[1],*
1 *ENSL, CNRS, Laboratoire de Physique, UMR 5672, F-69342 Lyon, France*
2 *Laboratoire Polymères et Matériaux Avancés, CNRS/Solvay, UMR 5268, 87 avenue des Frères Perret, 69192 Saint Fons Cedex, France and*
3 *Univ. Lyon, CNRS, INSA Lyon, Université Claude Bernard Lyon 1, MATEIS, UMR5510, 69100 Villeurbanne, France*
(Dated: July, 4th 2022)

We study by Dielectric Spectroscopy the molecular dynamics of relaxation processes during plastic flow of glassy polymers up to the strain hardening regime, for 3 different protocols of deformation. The measured dielectric spectra cover 4 decades in frequencies and allow us to measure the evolution as a function of the applied strain of the dominant relaxation time τ_α and of the width w_τ of the distribution of relaxation times.The first protocol is performed at constant strain rate $\dot{\lambda}$. We confirm that for increasing strain both τ_α and w_τ first decrease reaching a minimum in the stress softening regime before increasing in the strain hardening regime. In the second protocol we stop the deformation at some point λ_w in the strain hardening regime and we let the sample age for a waiting time t_w, during which the applied stress remains high. Upon resuming the deformation at constant $\dot{\lambda}$, stress-strain displays a yield stress and a stress softening regime comparable in magnitude to that of the reference protocol before rejoining the reference curve. In contrast the dielectric spectrum measured during the second protocol recovers the one measured during the reference curve much later than strain-stress. In the third protocol the stress is canceled during t_w. In this case after recovering the constant $\dot{\lambda}$ the dielectric spectrum and the stress-strain curve rejoin almost immediately the reference curve. We interpret these different behaviors as the consequence of changes in the free energy barriers for α-relaxation induced by the stress applied to the sample. These changes are the sum of two contributions: a) the first one, which allows for plastic flow, is due to the applied stress σ and, according to a recently published theory, scales as $-\sigma^2$; b) The second contribution $\kappa(\lambda)$, which is a function of the chain orientation at the monomer level, is positive and is responsible for the stress hardening regime. The first one evolves immediately upon varying the stress whereas the second relaxes very slowly upon cessation of the applied stress. Our interpretation for the results of the third protocol is that aging dynamics is frozen when the stress is removed, as it is known for polycarbonate at room temperature. Our experiments set precise conditions for a theory of strain hardening.

Keywords: polymer glass, relaxation time, dielectric spectroscopy, strain softening, plastic flow, strain hardening, aging process, Bauschinger effect, memory effect

I. INTRODUCTION

Mechanical and dynamical properties of polymers have been intensively studied for a long time, due to their fundamental and technological importance [1]. When strained at a given strain rate, beyond the elastic regime, glassy polymers exhibit a maximum in the stress-strain curves (yield point) at a strain of a few percents and typical yield stress values of a few tens of MPa's [2]. Beyond this maximum, depending on the history of the sample [3], the stress may drop by a few tens of MPa's (strain-softening regime) before it reaches a plateau corresponding to plastic flow. Strain-hardening (SH) may then occur at even larger strain, corresponding to an increase of the stress with strain, depending on molecular weight and cross-linking [4, 5].

Polymers can be brittle or ductile, with strain hardening occurring from a few tens of percent of true strain during tensile experiments. Strain hardening has been observed in highly entangled amorphous polymers such as polycarbonate (PC), poly(metyl)methacrylate (PMMA) or polyvinyl chloride (PVC) [6, 7]. It can be defined as a stress increase at high deformation [8–12] with a characteristic slope, called the strain hardening modulus (GR), of typical order of magnitude 10^7-10^8 Pa well below the glass transition [4, 13]. Strain hardening is essential for obtaining high mechanical properties, since this effect induces delocalization of the deformation and prevents the propagation of cracks and the formation of shear bands [5, 6, 14, 15].

Understanding deformation mechanisms of glassy polymers on the microscopic scale, from the linear regime up to the SH regime is an important and current scientific challenge. Over the past 20 years or so, many experiments with aim to identify and describe the microscopic mechanisms at play during plastic flow have been performed. One of the important features of the glass transition is the heterogeneous dynamics close to T_g [16, 17] which has been demonstrated experimentally over the past years by different techniques such as NMR [18], fluorescence recovery after photo-bleaching (FRAP) [19] or dielectric responses [20–22] among others. The characteristic size ξ of the dynamical

* caroline.crauste @ ens-lyon.fr, didier.long @ insa-lyon.fr

heterogeneities has been estimated by NMR [18] to be 3 to 4 nm at Tg + 20K in PVAc, as well as by theoretical arguments [23, 24]. Loo et al and Ediger et al [25–30] have studied the dynamics under plastic deformation by NMR and reorientation dynamics of small fluorescent molecular probes respectively. They have shown that the dynamics is strongly modified by the applied stress: it is accelerated even before the yield stress up to the stress softening regime and the onset of plastic flow. On the contrary, the dynamics is slowed down in the strain hardening regime [26–28]. They observed that the evolution of the width of the distribution of relaxation times is non monotonic. The width decreases first, and reaches a minimum at the end of the stress softening regime. Then, the width increases in the stress hardening regime. This effect is quantified with the Kohlrausch exponent β_K [26–28] which characterizes the width of the relaxation time distribution (RTD) and increases up to the onset of the strain hardening regime, during which it decreases. These effects have been confirmed by Dielectric Spectroscopy experiments [31–33].

The increase of the relaxation time upon stretching during the strain hardening regime appears to be a key feature of the microscopic mechanisms involved. Strain hardening had long been attributed, e.g. by Haward [8], to the entropic elasticity of an entangled or cross-linked rubbery network, an idea which was supported by experiments showing an increase of the hardening modulus with increasing entanglement or cross-linking densities. However more recent works by Govaert et al and by Hoy et al converge towards a different picture [6, 12, 34–36]. Van Melick and co-wokers have shown that the hardening modulus measured over a wide range of temperatures decreases linearly with temperature and becomes very small near the glass transition temperature, which goes against an entropic model. The recent experiments which have shown that the relaxation time increases in the SH regime also contradict this picture [26, 28, 33, 37]. The key new insights are that strain hardening appears to be controlled by the same mechanisms that control plastic flow [38] and the α-relaxation process on the monomeric scale, which are related to molecular interactions and are not directly related to chain conformation entropy.

On the theoretical side, a 3D mechanical model proved to be able to reproduce the viscoleastic properties of glassy polymers in the linear regime which showed that the relaxation times spectrum covers up to 8 decades [39, 40]. Regarding yield of glassy polymers, Chen and Schweizer described the plastic onset, yield and plastic flow with an approach similar in spirit to that of the energy landscape [41, 42]. At small deformation, the position of the system is slightly higher in the landscape, resulting in an accelerated dynamics. When the stress is relaxed, the system goes back down in its initial state. At higher strain, the free energy barriers are tilted and the system starts to flow. The change in free energy barrier as a function of the stress has a non zero slope at $\sigma = 0$ and is a convex function of σ. At a critical σ_c value, the barriers disappear altogether. Dequidt et al proposed that the decrease of the barriers is quadratic as a function of the applied stress and scales like $-\sigma^2$, the reduction corresponds to the stored elastic energy on the scale $\xi \sim 5nm$. The proposed model is able to estimate the evolution of the relaxation times distribution in 3D under any thermomechanical history in the linear and plastic flow regime, but without strain hardening. The physics introduced by Dequidt et al [43–45] has been confirmed quantitatively by Belguise et al. who accurately compared the model predictions with the stress relaxation function measured in the small amplitude plastic deformation regime [46].

Experiments aimed at determining how the distribution of relaxation times evolves in the plastic flow regime are thus crucially needed to make progress regarding the physical origin of stress hardening. Ediger at al. [29, 30, 47] add some small fluorescent molecular probes to polymer films under traction and measure their reorientation dynamics, getting access to the relaxation times distribution. It implies that the dynamics of the probe is strongly correlated to the one of the polymer. Dielectric spectroscopy (DS) allows to investigate the molecular dynamics of relaxation processes by means of the polarization of molecular dipoles on the polymer sample. This technique is directly sensitive to polymer mobility and it can be used to quantify the mobile fraction of polymer. Thus it is very convenient for the study of the microscopic mechanisms of plasticity. It has already been used in combination with mechanical deformation by Kalfus *et al* [31] and by the group of Ciliberto [32, 33, 37] during tensile experiments coupled with dielectric spectroscopy. We extend these studies to the strain hardening regime and also to memory effects in this regime. We consider various histories of deformation from the onset of the non-linear regime up to large amplitude deformation. We consider three deformation protocols. The first one is a constant strain rate protocole up to large amplitude of deformation (close to the breaking point of the sample). It allows us to describe how the distribution of relaxation times evolves from the linear regime, at yield, in the stress softening regime and then in the strain hardening regime. We show in particular that the dominant relaxation time evolves non-monotonically, a result already obtained by Lee *et al* [26, 27] and our group [33, 37]. Then we consider a second "relaxation protocol". We stop the deformation at some point during the strain hardening regime and maintain fixed the deformation. The stress remains high. We study the evolution of the distribution of relaxation times as well as that of the dominant relaxation time τ_α during this ageing step under non-zero stress. Then, we study the evolution of the distribution of relaxation times after resuming the deformation. We observe, as it

is known classically, that the second stress-strain curve recovers the reference one, which is a particular aspect of the so-called Bauschinger effect. We also observe that the distribution of relaxation times of the second curve also recovers that of the reference one. We study how these different curves rejoin the reference one as a function of the subsequent strain. We do similar studies in a third "unloading protocol" with the difference that the stress is set almost to zero during the arrest step. It allows us to compare ageing in the presence of an applied stress to ageing without stress, as well as the evolution of the relaxation time during ageing at zero stress to that during ageing with non zero stress.

We consider in detail the evolution of the distribution of relaxation times obtained by dielectric spectroscopy, and the evolution of the dominant relaxation time at the different steps of the applied deformation in all of the different stretching protocols. By extending already published theoretical works regarding the evolution of the free energy barriers in the presence of an applied stress, we show how our results allow us to explain, at a qualitative level, several specific features of the plasticity of polymers, from the onset of yield to the stress hardening regime, as well as several specific memory effects. We interpret these different behaviors as the consequence of changes in the free energy barriers for α-relaxation induced by the deformation applied to the sample. We propose that these changes are the sum of two contributions. The first one is negative and scales as $-\sigma^2$, where σ is the instantaneous value of the applied stress [43–46]. The second contribution $\kappa(\lambda)$, which is a function of the chain orientation at the monomer level, is positive and is responsible for the stress hardening regime [48]. The first one evolves immediately upon varying the stress whereas the second increases progressively upon applied strain and relaxes very slowly upon cessation of the applied stress.

The article is organized as follows. In section II the experimental set-up and methods are described. In section III, the measure of the dielectric properties is detailed during the three stretching protocols: the reference one, with continuous strain, the one with a stop at constant strain, and the one with a stop with released stress. In sections IV and V we discuss our results. We propose a physical interpretation for the results based on existing theories and propose how they may be extended in order to deal with strain hardening.

II. EXPERIMENTAL METHODS

First, we describe the sample properties, then the experimental setup. The setup is divided into two independent parts: the tensile machine and the dielectric spectrometer.

Samples: For the experiment, we have used commercial extruded polymer films MAKROFOL DE ®1-1 000000 based on MAKROLON ®polycarbonate (PC) from Bayer. The film thickness is 125μm and the glass temperature of about $T_g = 150°C$. Prior to test, each film is cut into a dog bone shape of size 42×21cm with a gauge width of 16.4cm. The films are in the deep glassy state since they are typically aged of several months or years and the experiment is performed at room temperature, which is far from the glass temperature.

Tensile Machine: The setup is composed of the uniaxial tensile machine that stretches the film until the failure. The film is attached to the two rollers of the machine with armed adhesive tapes. One of the two rollers is fixed and coupled to the load cell $2kN$ which measures the instantaneous force $F(t)$, whereas the other is movable and connected to the linear actuator so as to measure the film length $L(t)$ (inset Fig.1). The quantities of interest are the nominal stress $\sigma(t) = F(t)/S_0$, with $S_0 = 20.5mm^2$ the initial cross section of the sample, the strain $\lambda(t) = L(t)/L_0$ with L_0 the initial length and the strain rate $\dot{\lambda}$. Due to the presence of strain hardening in PC (high ductility), failure occurs for high strain of about $\lambda = 1.8 - 2$. Note that such high strain leads also to high variations of the film cross section which can make a substantial difference between the true and the nominal stress. The true stress is estimated by the formula $\sigma(t) = F\lambda^{2\nu}/S_0$ [48] with ν the Poisson's ratio of PC $\nu = 0.37$. Note that the Poisson's ratio may change during applied deformation. For a more quantitative value of the cross section, we refer to the work by Djukic et al [15] who measured the variation of the volume of PC samples during tensile strain deformation until breaking. Fig.1 shows that the true stress can be as high as 150% compared to the nominal stress at $\lambda = 1.8$. Moreover, we have checked that the sample deformation is homogeneous and there is no necking until the failure. To ensure the reproducibility of the data, each presented curve is the average of at least three tests.

Dielectric spectrometer: In parallel, the setup is equipped by a dielectric spectrometer which measures the complex permittivity $\epsilon^*(\omega) = \varepsilon'(\omega) - i\varepsilon''(\omega)$ of the film during the tensile test. In practice, the film is sandwiched and slides between two electrodes of 10 cm diameter. Since the film can undergo post-buckling at high deformation, we use an aqueous gel to facilitate the contacts. We have checked that its influence on the measurement can be neglected [49]: on the one hand the water absorption in PC films is weak ($< 0.2\%$) and on the other hand the electrical resistance of the gel is very low compared to the film. The electrodes are connected with the impedance analyzer that spans over 5 decades of frequency ranging from $10^{-2}Hz$ to 10^3Hz. Typically, the voltage signal applied to the electrodes is a $4V$ peak to peak periodic signal, composed of a dozen frequencies to ensure fast and precise impedance measurements at these frequencies. To get the impedance spectra, data are acquired at the sample frequency 8192 pts/s over a time window which depends on the strain rate. For ex-

ample, in case of the constant strain rate protocol with strain rate $\dot{\lambda} = 2.5 \times 10^{-4}\mathrm{s}^{-1}$ and a sample stretched from $\lambda = 1$ to $\lambda = 2$, the window is 64 s giving 60 independent segments and 110 segments with an overlap of 50% between each segment. For a faster strain rate ($\dot{\lambda} = 2.5 \times 10^{-3}s^{-1}$), the window must be shorter (5 s) because on one side, the segments length must be long enough to have access to the lowest frequency but on the other side not too long in order to correctly describe the dynamics as a function of strain. Finally, the data are processed with the Welch algorithm to get the spectra $\epsilon^*(\omega)$. More details on the procedure are given in Ref. [49].

The dielectric spectrometer provides the permittivities: $\varepsilon'(\omega) = Cd/(\varepsilon_0 S_E)$ and $\varepsilon''(\omega) = d/(\varepsilon_0 S_E R\omega)$ with d the film thickness, S_E the electrode surface, the resistance R and the capacity C of the film. In the following, we will mainly focus on the quantity: $\tan(\delta)(\omega) = \varepsilon''(\omega)/\varepsilon'(\omega) = 1/(RC\omega)$ which has the advantage to depend only on the dielectric material properties and not on the film thickness that can change during the tensile testing. Rheo-dielectrics measurements allow us to probe the molecular mobility of polymeric systems. Principles and main results for measurements at equilibrium around T_g are reviewed by Refs.[50, 51]. The extraction method for the mobility of the film from the $\tan(\delta)(\omega)$ spectra will be explained in Sec.III.1.

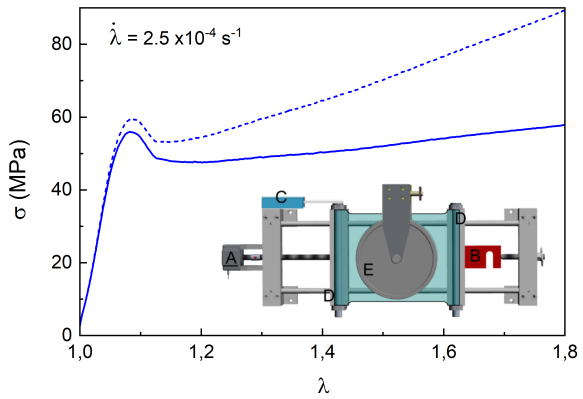

FIG. 1. Nominal stress (solid line) versus strain.Measured Young's modulus: $G' = 817MPa$. An estimation of the true stress (dashed line) is also indicated, see discussion. Inset: Sketch of the experimental setup. (A) motor, (B) cell load, (C) linear actuator, (D) sample fastening cylinders, and (E) electrodes for the dielectric measurement. The whole setup is enclosed in a Faraday cage to minimize low frequency electromagnetic perturbations coming from the outside.

III. MEASURE OF THE DIELECTRIC PROPERTIES

In order to investigate how the distribution of the relaxation times depends on the applied stress in the post yield regime, we propose to examine three different stretching protocols. The first is the constant strain rate protocol Sec.III.1, in which we explore the evolution of the main relaxation time τ_α and the stretching coefficient β (defined in Eq.1) as a function of strain. In particular these results will serve as a reference for analyzing two other more complex stretching protocols, presented in Secs.III.2, III.3. The purpose will be to study how the mobility is affected by the relaxation and the recovery after strain stops or stress unloading procedures.

III.1. Constant strain rate protocol

The first protocol investigated is the constant strain rate protocol, which consists in stretching the sample at constant strain rate from resting state until the failure. First, Fig.2(a) presents the stress-strain curve with $\dot{\lambda} = 2.5 \times 10^{-4}s^{-1}$, where four regimes can be distinguished: (i) The stress starts increasing up to the yield stress from $\lambda = 1$ to 1.08 (*Pre-yield*), (ii) then it decreases down from $\lambda = 1.08$ to 1.12 (*strain softening*), (iii) until it reaches a plateau from $\lambda = 1.12$ to 1.18 (*Plastic flow*). (iv) Finally for higher strain $\lambda > 1.18$, the stress increases again (*strain hardening*) until the film breaks.

Dielectric data have been recorded at the same time than the mechanical ones. Fig.2(a) shows the evolution of $\tan(\delta)$ at specific frequencies as a function of strain. What we see is that $\tan(\delta)$ evolves non monotonically at fixed frequency. At rest, $\tan(\delta)$ is around 1×10^{-3} at $0.125Hz$ with $\varepsilon'(0.125) \simeq 3$ and $\varepsilon''(0.125) \simeq 3 \times 10^{-3}$ (standard values in PC). Then at small strain, $\tan(\delta)$ increases and continues to do so until reaching a maximum value in the plastic flow regime ($\lambda = 1.12 - 1.18$) of about 17×10^{-3} at $0.125Hz$. This growth evidences an increase of the dissipation in the film. Then for higher strains corresponding to the strain hardening regime, $\tan(\delta)$ decreases down to the failure. In particular, we see that the evolution of $\tan(\delta)$ contrasts with the stress behavior. The maximum of $\tan(\delta)$ is reached after the yield stress, in the plastic flow regime. In the strain hardening there is a simultaneous increase of σ with the decrease of $\tan(\delta)$.

Note that in Fig.2(a), the variation of $\tan(\delta)$ is similar for all the plotted frequencies, except that higher amplitude variations of $\tan(\delta)$ are observed for lower frequencies. The effect can be better seen in the $\tan(\delta)(\omega)$ spectra. Fig.2(b) shows that only the low frequency behavior of the $\tan(\delta)(\omega)$ spectra in our frequency window ($10^{-2} - 10^{1}Hz$) is affected and rises during the stretching of the film. In particular, the elevation is the highest in the plastic flow regime ($\lambda = 1.12 - 1.18$) thus corroborated the evolution of $\tan(\delta)$ observed in Fig.2(a).

Extraction method for τ_α ***and*** β: We interpret [31–33] the rising of the $\tan(\delta)(\omega)$ spectra during stretching as the progressive shift of the α relaxation peak towards higher frequencies due to the mobility acceleration induced by plasticity, see Fig.2(b). More quantitatively,

we have shown in Ref. [33] that from these spectra, it is possible to estimate the mean relaxation time τ_α and the stretching coefficient β of the distribution of the relaxation times. In this section, we want to make use of the full potential of the method to discuss in detail the evolution of τ_α and β in the whole the post yield regime. As a reminder, the method uses the low frequency behavior of the $\tan(\delta)(\omega)$ spectra to probe the α relaxation process. In the typical Cole-Cole model for the α relaxation the $\tan(\delta)(\omega)$ spectra can be approximated in the limit case $\omega\tau_\alpha \gg 1$ by:

$$\tan(\delta) \simeq \frac{\Delta sin(\beta\pi/2)}{(\omega\tau_\alpha)^\beta}. \quad (1)$$

where $\Delta = (\epsilon_0 - \epsilon_\infty)/\epsilon_\infty$ is the dielectric strength, τ_α the main relaxation time and β the stretching exponent.

The method consists in fitting the low frequency behavior of $\tan(\delta)(\omega)$ in our frequency window and extract the parameters. However, they cannot be determined all together because, as it can be seen in Fig.2(b), the relaxation peak does not show up completely in the frequency window. More precisely, the extraction gives β and an intermediate relaxation time τ_{eff} that depends on τ_α and Δ so that it is possible to infer τ_α only by assuming the value of Δ and its constancy all along the test. We recognize that the method does not directly provide the main relaxation time τ_α but it gives at least a relevant estimation.

Although not straightforward, the interpretation of the rising of the $\tan(\delta)(\omega)$ spectra as a consequence of mobility acceleration is supported by several evidences which have been discussed in details in previous studies [31–33]. For example, one important fact is that the rising of the $\tan(\delta)(\omega)$ spectra during stretching and at any λ looks qualitatively similar to the one caused by the mobility acceleration as the system is heated close to T_g. The similarity has been observed for different types of polymer glasses (PVC or PC) either for $\tan(\delta)(\omega)$ or for other dielectric quantities such as $\varepsilon'(\omega)$, see Ref. [31–33]. A A-type dipole polymer has his dipoles along the chain. Our polycarbonate sample is a B-type dipole polymer for which dipoles are carried on pendant groups [52]. Indeed, we did not observe any peak at lower frequencies in the high temperature range other than the one corresponding to the α-relaxation process.

Moreover, we have shown in Ref. [33] that the large increase of the $\tan(\delta)(\omega)$ spectra with the strain rate $\dot{\lambda}$ ranging four decades $10^{-6}s^{-1} < \dot{\lambda} < 10^{-3}s^{-1}$ is much more compatible with a tremendous increase of τ_α satisfying the scaling law $\tau_\alpha \simeq 1/\dot{\lambda}$ rather than an unlikely increase of Δ up to a factor of 100. Even if we do not exclude that the dielectric strength Δ may vary by a factor of the order of a few units during the stretching, this variation alone cannot be enough to justify the evolution of τ_α covering several orders of magnitude. Then, the estimation of τ_α should not be so far from the reality.

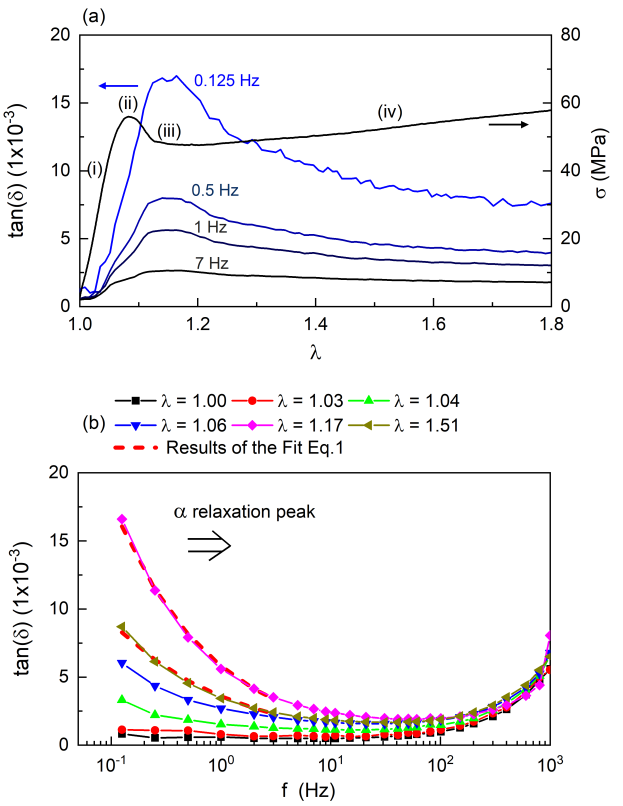

FIG. 2. (a) $\tan(\delta) = \varepsilon''/\varepsilon'$ (Left axis) at several frequencies $\{0.125, 0.5, 1, 7\}Hz$ and nominal stress σ (Right axis) as a function of strain for the constant strain rate protocol with $\dot{\lambda} = 2.5 \times 10^{-4}s^{-1}$. (b) $\tan(\delta)(f)$ spectra pick up at several strains. In red dashed line, two examples of fit with Eq.1 for $\lambda = 1.17$ and $\lambda = 1.51$.

A possible value of Δ can be obtained from the temperature measurement of Ref. [32] made on the same PC film, where we have measured $\Delta = 0.125$ at $T = 152°C$. With this value, one can get an estimation of τ_α: For example, at $\lambda = 1.17$, the numerical application gives $\tau_\alpha \simeq 40s$ and $\beta \simeq 0.5$. In Fig.3 and Fig.4, we apply systematically the method to extract τ_α and β as a function of strain λ for the constant strain rate experiment with two different strain rates $\dot{\lambda} = 2.5 \times 10^{-4}s^{-1}$ and $\dot{\lambda} = 2.5 \times 10^{-3}s^{-1}$.

Evolution of τ_α: The variation of $\tan(\delta)$ at fixed frequency observed in Fig.2(a) with $\dot{\lambda} = 2.5 \times 10^{-4}s^{-1}$ can be therefore understood and converted into a non-monotonic variation of the main relaxation time τ_α. This novel perspective shall allow us to better characterize the deformation regimes at work in PC, see Fig.3(a). Interestingly, the four regimes described above in term of stress remain also relevant when considering the evolution of τ_α: (i) *Pre-yield*: the stress and the mobility both increase, (ii) *strain softening regime*: the stress decreases whereas the mobility continues to grow, (iii) *plastic flow*: the stress and the mobility reach a plateau and finally

(iv) *strain hardening*: the stress increases again whereas the mobility decreases.

The variations at low frequencies in $\tan(\delta)$ are also sensitive to strain rate [31–33] so that the extracted value τ_α should also depend on it. To confirm this dependance, we reproduce the experiment with a strain rate one decade faster $\dot{\lambda} = 2.5 \times 10^{-3} s^{-1}$. Fig. 3(b) shows that the evolution of the dimensionless parameter $\tau_\alpha \dot{\lambda}$ with λ, collected at different strain rates, collapse in a single curve. In other terms, the extracted τ_α follows an approximate $1/\dot{\lambda}$ scaling law, valid for the entire post yield regime of the polymer glass. Interestingly the value of $\tau_\alpha \dot{\lambda}$ reaches about 10^{-2} in the plastic flow regime ($\lambda \sim 1.12 - 1.18$), which is comparable to the value reported in the plastic flow of Poly(methyl methacrylate) (PMMA) glass obtained with the molecular probe reorientation experiment [53]. Benefiting from the high ductility of PC, Fig. 3(b) also shows the influence of the strain hardening on the dynamics. For example, in the range of $1.18 \leq \lambda \leq 1.8$, the quantity $\tau_\alpha \dot{\lambda}$ monotonically increases by a factor of ten. Therefore, the global effect of the strain hardening is to slow down the mobility while holding a scaling law of type $\tau_\alpha \simeq 1/\dot{\lambda}$ until the failure of the film.

Evolution of β: Besides the dominant relaxation time, the extraction also provides the stretching exponent β that quantifies the width of the distribution of relaxation times. An increase of β corresponds to a narrowing of the distribution, and a decrease to a broadening of the distribution. The comparison between Fig.3(a) and Fig.4(a) shows that β is correlated with τ_α in all regimes of deformation. A faster mobility (decrease of τ_α) tends to homogenize the dynamics (increase of β). For example in Fig.4(a), the mobility through τ_α and the stretching exponent β both increase in the stress softening regime (ii) and reach a maximum in the plastic flow (iii), with a maximum for β of about 0.5. Then, the mobility and β decrease in the strain hardening regime (iv). From our measurement, we also note that β ranges between $0.4 - 0.5$ in the entire post yield regime, see Fig.4(a), which is systematically above the value measured at fix temperature for which β is much closer to $0.2 - 0.3$ in the range $130°C - 170°C$ [32]. It means that while the mobility of the stretched film increases towards the plastic state, similarly to a heating near T_g, the dynamics under stress is on the contrary much more homogenized. Therefore, we conclude from dielectric measures that: (1) the mobility is positively correlated with the homogeneity of the polymer dynamics under stretching and (2) stretching is not strictly equivalent to heating. This fully supports similar conclusions made earlier by mechanical [54] or by molecular probes experiments [26, 55]. Theoretically, the models of Refs.[41, 43, 44] account for this effect.

In Fig.4(b), the relation between β and τ_α can be made even more precise. We observe for the constant strain rate experiments that β is linearly correlated with $ln(\tau_\alpha)$ in all post yield regimes. The relation holds either for

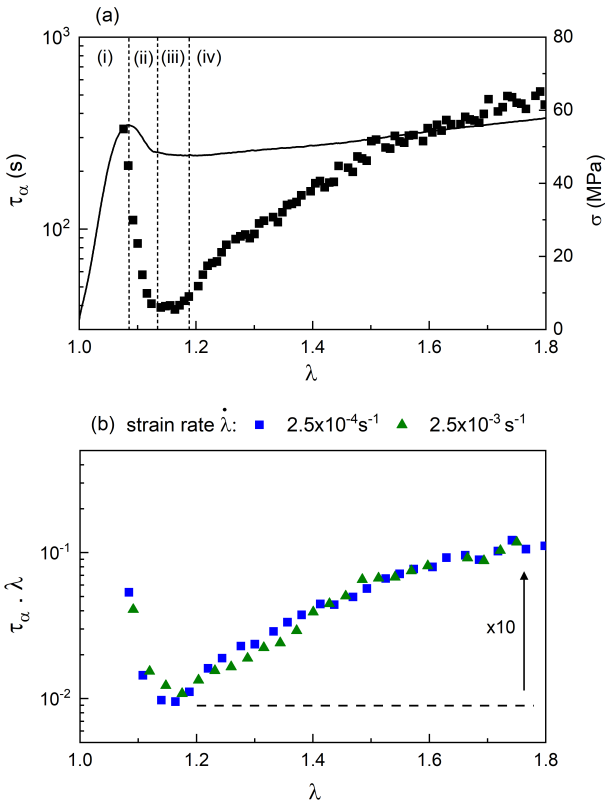

FIG. 3. (a) Mean relaxation time τ_α (Left axis, dots) and nominal stress σ (Right axis, line) as function of strain for $\dot{\lambda} = 2.5 \times 10^{-4} s^{-1}$. (b) Dimensionless parameter $\tau_\alpha \dot{\lambda}$ as function of strain for the two strain rates indicated. τ_α and β are extracted with the dielectric strength $\Delta = 0.125$. The same value of Δ is used in the rest of the article.

$\dot{\lambda} = 2.5 \times 10^{-4} s^{-1}$ or for $\dot{\lambda} = 2.5 \times 10^{-3} s^{-1}$, the slopes being almost the same (not shown here). In particular, this supports recent results of Ediger and coworkers [26, 30] obtained in stretched PMMA and PLA glasses by molecular probe experiments. A similar relation with a material dependent slope is found, so that it is highly probable that the slope depends also on the material in our case, although we did not test it. Moreover, it should be noted that the relation $\beta \propto ln(\tau_\alpha)$ holds for any protocols and when the relaxation time either increases or decreases during the constant rate experiment. In the relaxation and unloading protocols presented in Secs.III.2, III.3, the relation is retrieved either before the waiting steps, or after once the strain rate resumes (at $\dot{\lambda} = 2.5 \times 10^{-4} s^{-1}$). This can be viewed in Fig.4(b) where we see that the data obtained for the three protocols overlap each other. For this reason, the relation may be quite universal and should reflect an important feature of the plasticity. The evolution of τ_α and β especially in the strain hardening regime, will be further interpreted in Sec.IV.1.

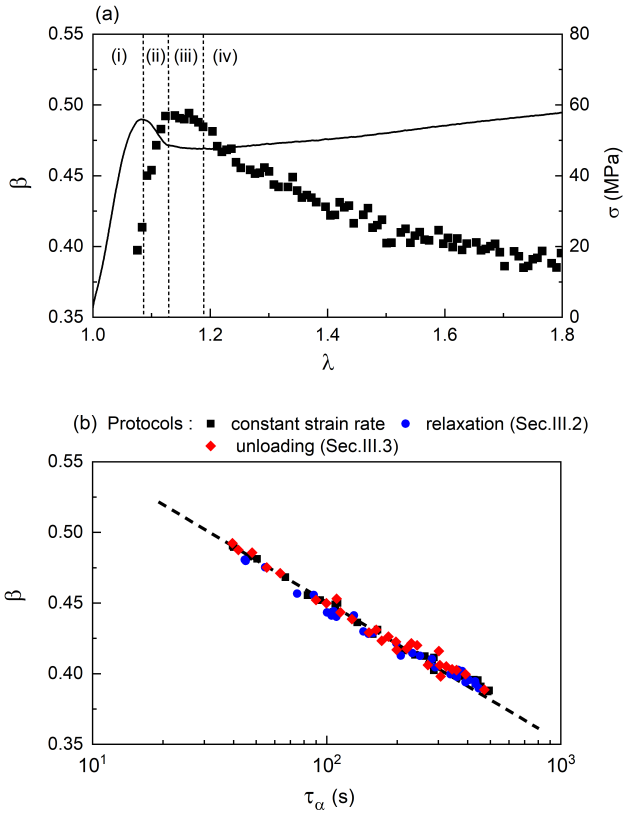

FIG. 4. (a) Stretching parameter β (Left axis, dots) and nominal stress σ (Right axis, solid line) at $\dot{\lambda} = 2.5 \times 10^{-4} s^{-1}$ as function of strain. (b) Relation between β and τ_α observed for different protocols: The constant strain rate protocol at $\dot{\lambda} = 2.5 \times 10^{-4} s^{-1}$. The relaxation protocol discussed in Sec.III.2 with $\lambda_w = 1.2$, $t_w = 1h$ and $\dot{\lambda} = 2.5 \times 10^{-4} s^{-1}$. The unloading protocol of Sec.III.3 with $\lambda_p = 1.25$, $\lambda_w = 1.2$, $t_w = 1h$ and $\dot{\lambda} = 2.5 \times 10^{-4} s^{-1}$. Note the log scale for the x-axis.

III.2. Relaxation protocol

In this section, we address the relaxation protocol in which a waiting (aging) step is inserted in the middle of a constant strain rate experiment (called reference in the following), see Fig.5(a). First, the stretching of the film starts at $\dot{\lambda} = 2.5 \times 10^{-4} s^{-1}$ (i-initial step), then the strain rate stops $\dot{\lambda} = 0 s^{-1}$ in the post yield regime (ii-waiting step) at a specific strain λ_w, and during a specific time t_w. For example, the waiting strain values λ_w investigated are either in the plastic flow / onset of strain hardening $\lambda_w = 1.2$ or in the strain hardening regime $\lambda_w = 1.5$. Regarding the waiting time t_w, the values can be $t_w = 100s$, $t_w = 1h$ or $t_w = 62h$. Once the time is elapsed, the strain rate resumes at the same initial strain rate (iii-recovery step). In particular, we will focus only on one value of strain rate $\dot{\lambda} = 2.5 \times 10^{-4} s^{-1}$.

Figs.5(b,c) show the temporal evolution of the stress $\sigma(t)$ and the dielectric $\tan(\delta)(t)$ at specific low frequencies during the experiment, with the aging parameters $\lambda_w = 1.2$ and $t_w = 1h$. The variation of the low frequencies of $\tan(\delta)$ is again very important, reflecting the variation of the mobility and therefore the distribution of the relaxation times. It is possible to extract τ_α and β with the extraction method previously discussed and show that τ_α and β follow the same correlation as in the reference protocol Fig.4(b). For this reason, we shall discuss only the evolution of τ_α during the experiment Figs.5(d), since β can be directly deduced from it. The following behaviors are identified, see Fig.5(b-d). During the initial step $\lambda < \lambda_w$, the evolutions of σ, $\tan(\delta)$ and τ_α are identical to the ones observed in the reference protocol: the stress undergoes a yield stress and decreases as strain approaches $\lambda_w = 1.2$, while $\tan(\delta)$ and the mobility increase and reach a maximum. During the waiting step starting at $\lambda_w = 1.2$ and time t_i, σ, $\tan(\delta)$ and the mobility both decrease. Finally during the recovery step which starts at $t_f = t_i + t_w$, the stress σ, $\tan(\delta)$ and the mobility start rising again. After a transitory period, we see that all the quantities recover their reference values as if no stop had occurred. For completeness, we show in Fig.6 the corresponding evolution of the $\tan(\delta)(\omega)$ spectra during the experiment.

Recovery step: We focus on the recovery step $\lambda > \lambda_w$ of the relaxation protocol, from the resumption of the strain rate and until the film breaks. Fig.7 shows the behavior of the three observables : the stress σ, the dielectric $\tan(\delta)$ at $0.125Hz$ and the relaxation time τ_α, compared with their reference behaviors, as a function of the strain λ. On the one hand, we see that all the properties of the film converge to their reference behaviors. On the other hand we also see that different values of aging parameters, λ_w and t_w, can drastically influence the recovery dynamics. In the following, we denote the recovery strain λ_{rc} at which the properties recover their reference curves after the beginning of the resumption.

First, Fig.7(a,c,e) show the result for $\lambda_w = 1.2$. When looking at $\lambda > \lambda_w$ and at fixed t_w (for example $1h$), the three responses increase toward their reference behaviors exhibiting a temporary overshoot above the reference curve before relaxing to it. Therefore, all the responses are found to be non monotonic. However, note the following differences according to the observable. In case of the stress σ in Fig.7(a), the overshoot peak is well defined with a strong and sharp peak while in the case of $\tan(\delta)(0.125)$ in Fig.7(c), the peak is much broader and weaker. Another important difference lies in the time occurrence of the overshoot peak. In case of the stress, the peak occurs very soon after the resumption so that the stress is most of the time situated above the reference curve during the recovery step, while in case of $\tan(\delta)(0.125)$ the peak occurs much later in time so that the responses are below the reference curves during a much longer period.

Figs.7(a,c,e) show the influence of t_w. We see that the three responses σ, $\tan(\delta)$ and τ_α rejoin their reference behaviors after a longer delay as t_w increases, so that the

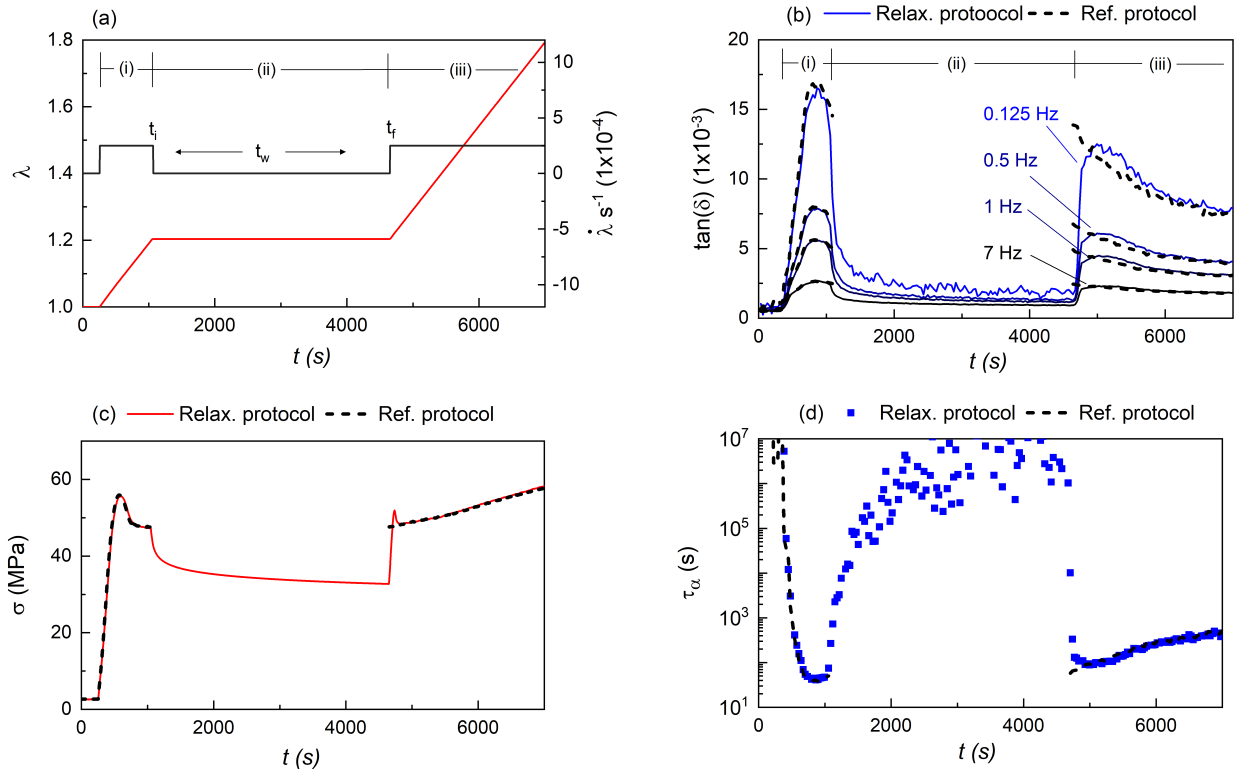

FIG. 5. Description of the relaxation protocol with $\lambda_w = 1.2$, $t_w = 1h$ and $\dot{\lambda} = 2.5 \times 10^{-4} s^{-1}$ (if not zero). (a) Time evolution of strain $\lambda(t)$ (Left axis, red line) and strain rate $\dot{\lambda}(t)$ (Right axis, black line) during the whole experiment. t_i and t_f delimit the beginning and the end of the pause step of duration $t_w = t_f - t_i$. (b-d) Time evolution of the stress $\sigma(t)$ (b), the dielectric $\tan(\delta)(t)$ at several frequencies $\{0.125, 0.5, 1, 7\} Hz$ (c) and the mean relaxation time τ_α (d) during the relaxation protocol (a). τ_α is extracted following the method of Sec.III.1 with $\Delta = 0.125$. In black dashed lines, reference curves obtained at constant strain rate $\dot{\lambda} = 2.5 \times 10^{-4} s^{-1}$ for comparison purpose (same as Fig.2). On top of (a) and (b), the three steps of the protocol are indicated: (i) initial,(ii) waiting and (iii) recovery steps.

recovery dynamics is slowed down. For example in case of σ, the recovery strains are $\lambda_{rc} = 1.23, 1.25, 1.42$ at $t_w = 100s, 1h, 62h$, arrows in Fig.7(a) and in case of $\tan(\delta)$ (or τ_α), $\lambda_{rc} = 1.23, 1.45, 1.65$ at $t_w = 100s, 1h, 62h$, arrows in Figs.7(c,e). The slow down of the recovery dynamics is caused by the film aging during the waiting step, which is a well-known feature reported since the 1960s [56, 57]. In particular, Kramer [57] showed with a similar protocol applied to Nylon, that the amplitude and time of the recovery response of the stress σ scale with $ln(t_w)$. Similarly, the overshoot peak of the stress in Fig.7(a) delays as well as grows in amplitude as t_w increases. We have also checked that the logarithmic relation is verified in our case (not showed). Moreover, the Young's modulus G' at the resumption also increases with t_w: $G' = 989, 1091, 1180 MPa$ at $t_w = 100s, 1h, 62h$, which is another consequence of the film aging.

Interestingly, the slow down of the recovery dynamics can also be observed for the dielectric quantity $\tan(\delta)(0.125)$ Fig.7(c). An increase of t_w increases the amplitude and delays the overshoot peak as for the stress. More precisely, it is even possible to scale the response of $\tan(\delta)(0.125)$ by $ln(t_w)$, as we discussed it in Ref.[37]. The scaling proves to be efficient for large t_w such as $t_w = 1h$ and $t_w = 62h$ and works either for $\lambda_w = 1.2$ and for $\lambda_w = 1.5$. This new sensitivity to t_w in terms of the mobility through the dielectric variables, in addition to stress, evidences a long term memory of the past mechanical history.

In addition, Figs.7(b,d,f) show the recovery dynamics after aging in the full strain hardening regime $\lambda_w = 1.5$. As in the case $\lambda_w = 1.2$, similar features can be noticed such as the non monotonic responses of σ, $\tan(\delta)(0.125)$ and τ_α or the slowing down of the recovery with the increase of the waiting time t_w. Note that here, the overshoot of $\tan(\delta)(0.125)$ at $t_w = 62$ h is barely seen because it occurs presumably at deformations larger than the breakdown. Note also that τ_α rejoins the reference curve at a very late stage. One major difference compared to $\lambda_w = 1.2$ is that the recovery dynamics at $\lambda_w = 1.5$ is much slower for a same t_w, which can be observed on the dielectric variables $\tan(\delta)(0.125)$ and τ_α, see Figs.7(d,f). Actually, the difference is quite sensitive. At $\lambda_w = 1.2$ and $t_w = 1h$, the recovery of $\tan(\delta)(0.125)$

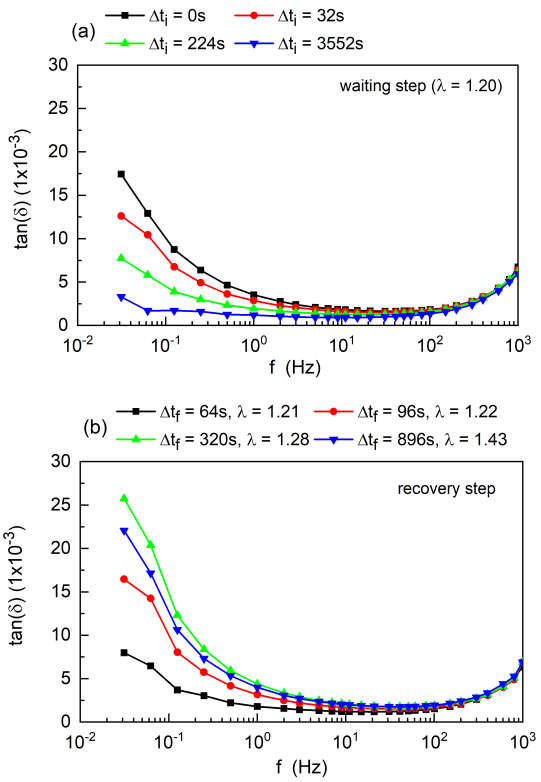

FIG. 6. Dielectric $\tan(\delta)(f)$ spectra for the experiment of Fig.5. (a) During the waiting step at $\lambda_w = 1.2$ and at several times $\Delta t_i = t - t_i$ elapsed since the beginning of the waiting step. (b) During the recovery step at several strains. We also indicate the corresponding time $\Delta t_f = t - t_f$ elapsed since the beginning of the recovery step.

and τ_α to the reference curve occurs around $\lambda_{rc} = 1.45$ (equivalent to $t - t_f = 980s$) after the resumption of the strain rate, while at $\lambda_w = 1.5$ and $t_w = 1h$, the recovery occurs much later after the breakdown $\lambda_{rc} > 1.85$ ($t - t_f > 1400s$). Such influence of λ_w on the dynamics echoes previous observations made regarding the mobility recovery after multi creep deformation [27]. The authors show with molecular probe experiments, that mobility takes a longer time to recover the reference after an arrest in the strain hardening. This is the other side of the same phenomenon. Hence, the results evidence that the recovery processes after aging at high level of stress depend on the waiting time t_w as much as the waiting strain λ_w. In particular, the latter dependence may be explained by the possible contribution of the strain hardening. An interpretation is given in Sec.IV.3.

III.3. Unloading protocol

The last protocol studied is the unloading protocol [58], in which the polymer film is allowed to retract before starting the pause interval. Compared to the relaxation protocol of Sec.III.2, the main difference is that now the pause interval is achieved at considerable lower stress. Then the purpose is to identify what will be the influence of the retraction step on the subsequent dynamics of the mechanical and dielectric observables, in particular when the strain rate will resume.

The unloading protocol is described in Fig.8(a). First, the film is stretched with the strain rate set to $\dot{\lambda} = 2.5 \times 10^{-4}\ s^{-1}$ (i-initial step). Then at the deformation λ_p and time t_p, the strain rate is reversed ($\dot{\lambda} = -2.5 \times 10^{-4} s^{-1}$) so that the deformation decreases (ii-retraction step). When reaching λ_w at time t_i, the strain rate stops and the pause interval of duration t_w begins (iii-waiting step). For comparison purposes, we choose the same waiting parameters in the pause λ_w and t_w as those in the relaxation protocol, either $\lambda_w = 1.2$ or $\lambda_w = 1.5$ for the waiting deformation, and either $t_w = 1h$ or $t_w = 62h$ for the waiting time. Finally at t_f, the strain rate resumes at the same initial strain rate until the film breaks (iv-recovery step). As in Sec. III.2, all the experiments performed are carried out with the same strain rate $\dot{\lambda} = \pm 2.5 \times 10^{-4} s^{-1}$. Note that in the reverse step, the stretched polymer retracts itself because the film inherently wants to come back to equilibrium to discharge its elastic component. The deformation limit λ_p before reversing depends on λ_w and it is chosen in such a way that the stress drops by a factor 10 during the retraction. Therefore λ_p is not necessarily the same for $\lambda_w = 1.2$ or $\lambda_w = 1.5$. For example, we choose $\lambda_p = 1.25$ and $\lambda_p = 1.57$ respectively in case of $\lambda_w = 1.2$ and $\lambda_w = 1.5$. Ideally, we would have wanted to completely remove the stress but a residual stress is needed to maintain the setup operational for the rest of the protocol. However, this residual stress does not change the results and therefore it will be neglected in what follows.

As an example, the time evolution of the stress σ and the dielectric $\tan(\delta)$ at several frequencies are plotted in Fig.8(a-b) during the unloading protocol with the parameters $\lambda_p = 1.25$, $\lambda_w = 1.2$ and $t_w = 1h$. Fig.9 shows the corresponding $\tan(\delta)$ spectra. Again in this protocol, the variation of the low frequencies of $\tan(\delta)$ can be interpreted in terms of a variation of the mobility (Fig.8(b,d)). As with the other protocols, τ_α and β follow the same correlation, see Fig.4(b). The three following behaviors are identified. During the initial step $\lambda < \lambda_p$, σ, $\tan(\delta)(0.125)$ and τ_α evolve as in the reference protocol of Sec.III.1. During the retraction step, the stress decreases over time. Compared to the relaxation protocol, the decrease is controlled by the strain rate. In contrast, we can see that the behavior of $\tan(\delta)$ and τ_α are more complex. $\tan(\delta)$ first decreases and then stabilizes to an intermediate value, as evidenced by the resurgence occurring around $t = 1500s$, see Fig.8(b). In terms of relaxation time Fig.8(d), it means that the retraction step temporarily stops the aging process and holds the mobility at a non equilibrium value. In Fig.8(c) we observe a slow increase of the stress over several thousands of seconds while the deformation is maintained fixed before the stress eventually levels off. This effect is a classical

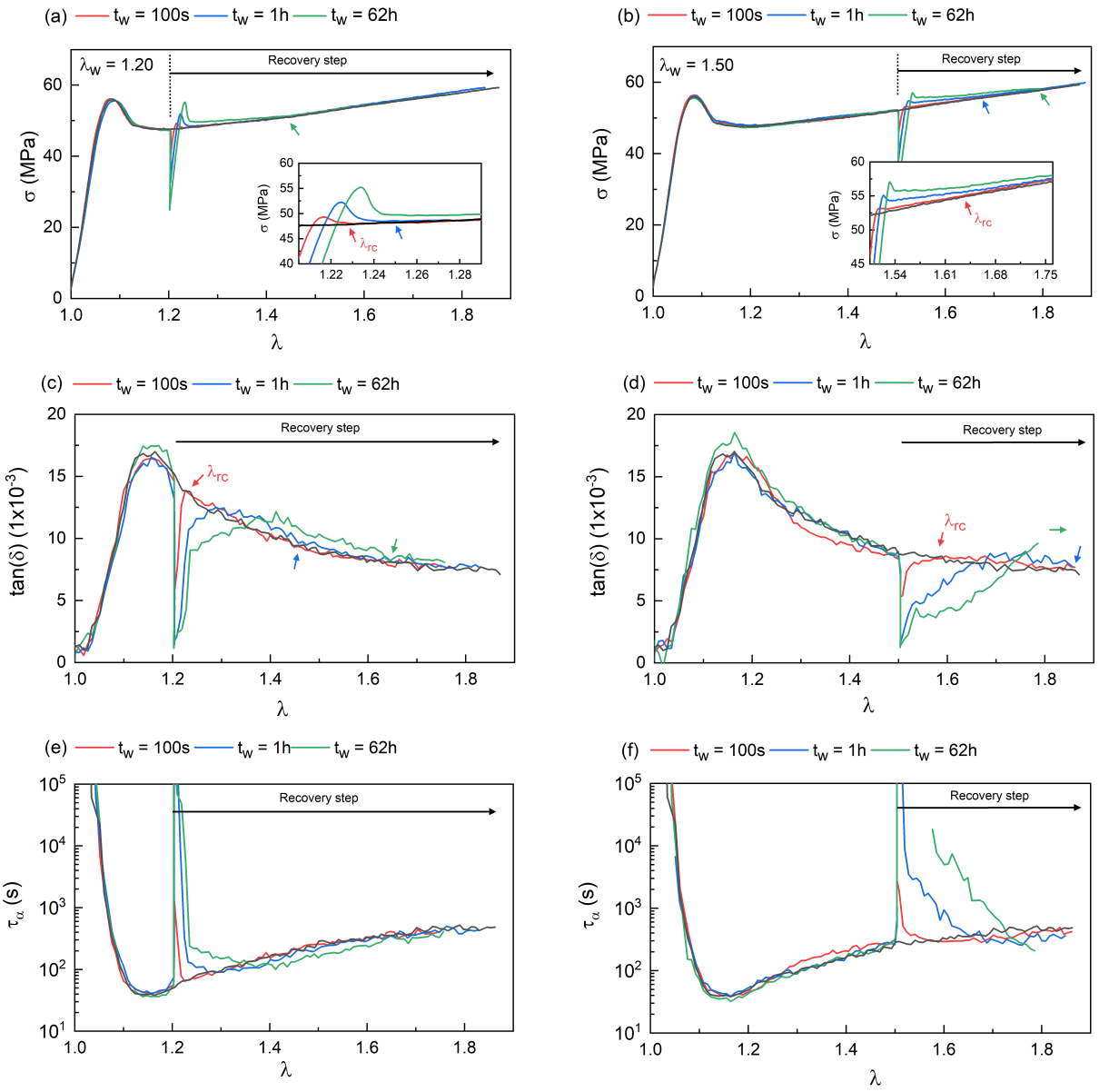

FIG. 7. Relaxation protocols with $\lambda_w = 1.2$ (a,c,e) and $\lambda_w = 1.5$ (b,d,f) for different waiting times $t_w = 100s, 1h, 62h$. Evolution of stress σ (a,d), $\tan(\delta)$ at $0.125Hz$ (b,e) and relaxation time τ_α (c,f) as function of strain λ. In black line, the reference curves.The arrows mark the recovery strains λ_{rc} at which the properties recover their reference curves after the beginning of the resumption (same for $\tan(\delta)$ and τ_α).

viscoelastic effect [1, 59] when one prevents subsequent shape relaxation of a polymer sample after that the sample is allowed to relax at zero stress for a while. Interestingly, one observes the simultaneous decrease of $\tan(\delta)$ and of the mobility. We have checked that the evolution of σ, $\tan(\delta)(0.125)$ and the mobility are logarithmic processes (not shown here). During the recovery step and the resumption of the strain rate, σ, $\tan(\delta)$ and the mobility increase again so as to recover their reference values as if no stop had occurred. ***Recovery step***: We focus on the recovery dynamics and ask, whether or not, different waiting parameters λ_w and t_w can change the recovery responses, in a way similar to what has been observed in the relaxation protocol of Sec. III.2. Fig.10 summarizes the results, by showing the stress σ, the dielectric $\tan(\delta)$ and the relaxation time τ_α, as a function of strain λ for different unloading protocols with various waiting parameters λ_w and t_w. The reference curves are in black so as to study the recovery responses. In contrast to the relaxation protocol, we see that the recovery responses in the unloading protocol are much less sensitive to the waiting parameters. For example, an increase of the waiting time

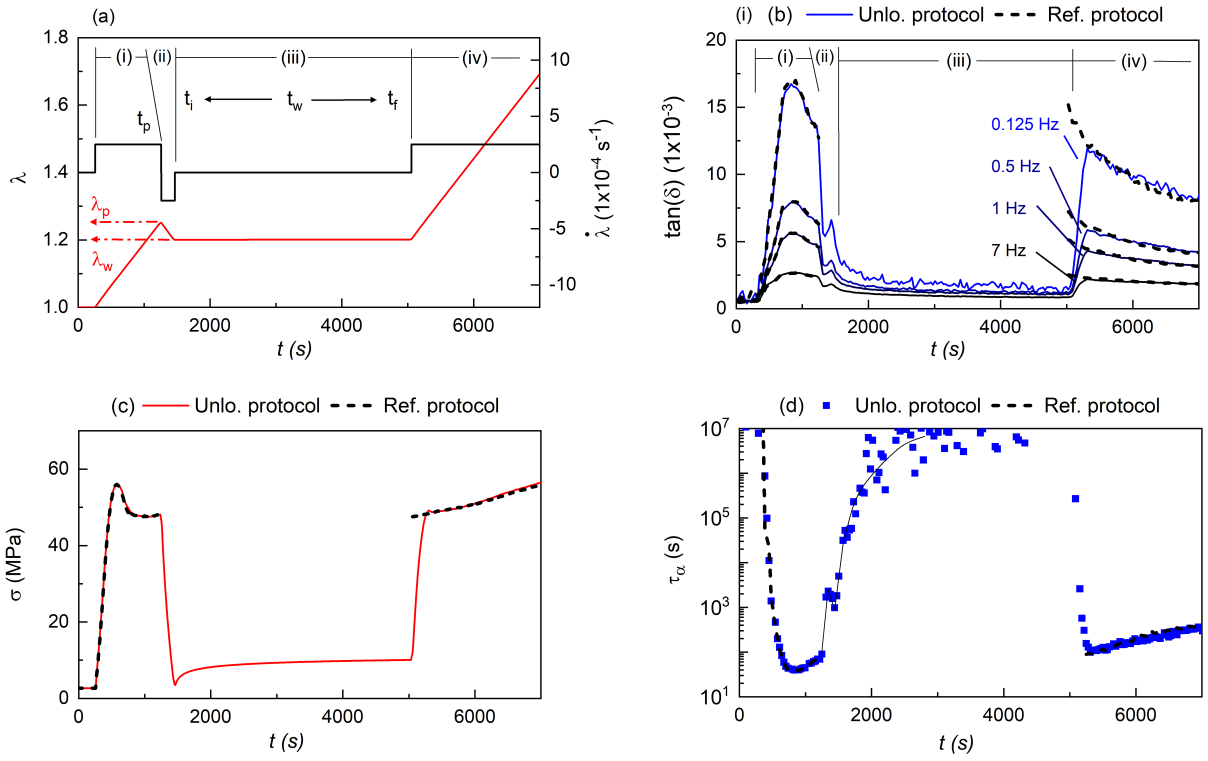

FIG. 8. Description of the unloading protocol with $\lambda_p = 1.2$, $\lambda_w = 1.2$, $t_w = 1h$ and $\dot{\lambda} = \pm 2.5 \times 10^{-4} s^{-1}$ (if not zero). (a) Time evolution of strain $\lambda(t)$ (Left axis, red line) and strain rate $\dot{\lambda}(t)$ (Right axis, black line) during the whole experiment. t_i and t_f delimit the beginning and the end of the waiting step of duration $t_w = t_f - t_i$. t_p mark the beginning of the retraction step. (b-d) Time evolution of the stress $\sigma(t)$ (b), the dielectric $\tan(\delta)(t)$ at several frequencies $\{0.125, 0.5, 1, 7\} Hz$ (c) and the mean relaxation time τ_α (d) during the relaxation protocol (a). In black dashed lines, reference curves obtained at constant strain rate $\dot{\lambda} = 2.5 \times 10^{-4} s^{-1}$ for comparison purpose (same as Fig. 2). On top of (a) and (b), the four steps of the protocol are indicated: (i) initial,(ii) waiting, (iii) retraction and (iv) recovery steps.

has practically no influence neither on the stress σ nor on the dielectric variables $\tan(\delta)$ and τ_α. In Fig.10(a), the stress response σ at fixed $\lambda_w = 1.2$ exhibits a weak overshoot for $t_w = 62h$ and for $t_w = 1h$, but the amplitudes are eventually much smaller than those observed in the relaxation protocol. At the opposite, it even appears that a longer waiting time slightly advances the overshoot peak. Moreover, the recovery responses $\tan(\delta)$ and τ_α in Figs.10(b-c) do not exhibit any distinguishable overshoots nor supplementary recovery delay. Besides t_w, we see that the waiting deformation λ_w has also little influence on the recovery dynamics. For example at fixed $t_w = 1h$ and for different λ_w, Figs.10(a-c) shows that σ, $\tan(\delta)$ and τ_α behave the same regardless the value of λ_w. The behavior of the recovery responses in the unloading protocol is in total opposition with the relaxation protocol, for which the waiting parameters t_w and λ_w were determinant.We come back to this point in Sec.IV.4.

IV. PHYSICAL INTERPRETATION

IV.1. General observations

We discuss here the physical interpretation of our results following the same outline as the experimental part. We start by recalling that our samples have aged for a long time since they have been prepared, and that, after a temperature quench, ageing corresponds to a progressive increase of the dominant relaxation time associated to a progressive densification of the polymer [60, 61]. We first consider the reference protocol and more specifically the results presented in Figures 2 and 3. The main observation is the non-monotonic evolution of the dominant relaxation time. The latter first decreases. Note that it starts decreasing even before yield as it has been observed in earlier experiments [25–28]. In Figure 3 the first results of our experiments start at yield, for which the dominant relaxation time is 300 s, whereas the initial relaxation time before deformation may be estimated to be at least of the order of 10^6 s [61]. The

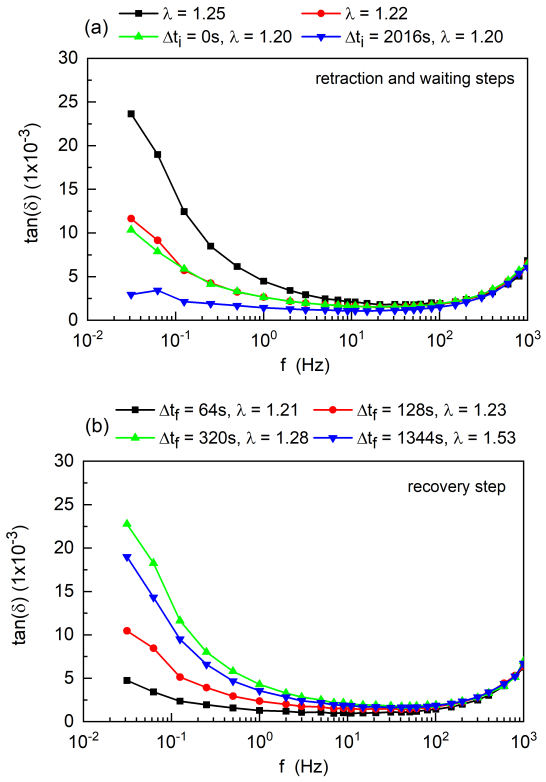

FIG. 9. Dielectric $\tan(\delta)(f)$ spectra for the experiment of Fig.8. (a) During the retraction and the waiting steps. For the waiting step at $\lambda_w = 1.2$, the time $\Delta t_i = t - t_i$ elapsed since the beginning of the waiting step is given. (b) During the recovery step at several strains. We also indicate the corresponding time $\Delta t_f = t - t_f$ elapsed since the beginning of the recovery step.

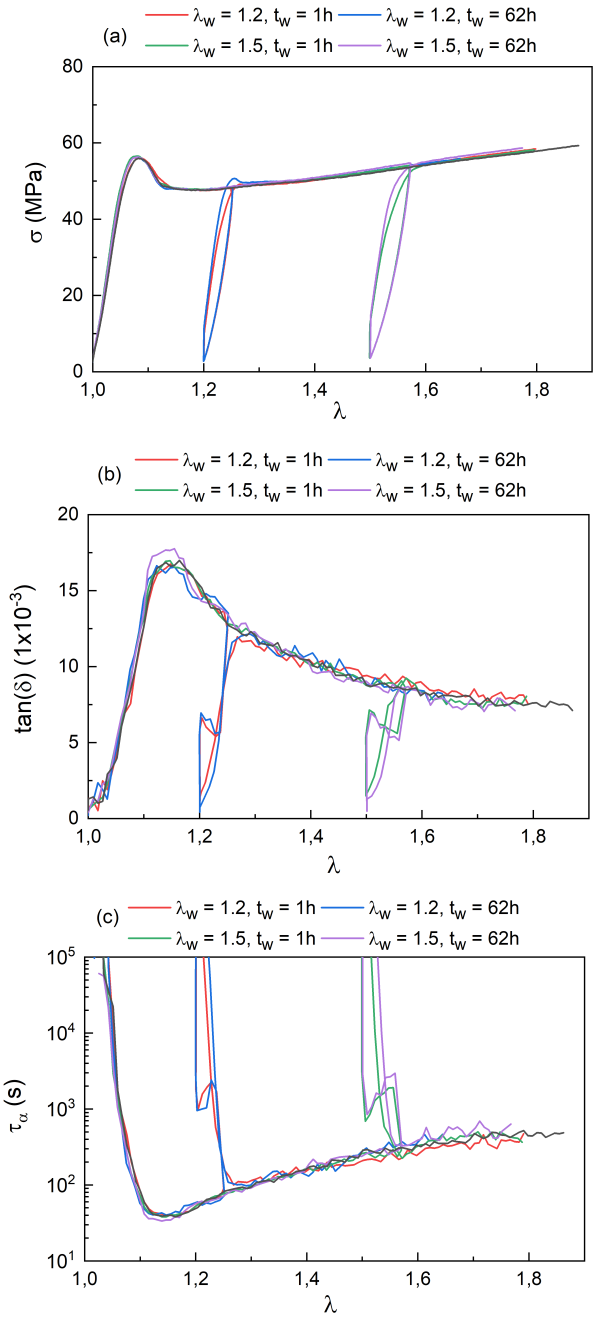

FIG. 10. Unloading protocols with $\lambda_p = \{1.25, 1.57\}$, $\lambda_w = \{1.20, 1.50\}$ and $t_w = \{1, 62\}h$. (a) Stress σ, (b) $\tan(\delta)$ at $0.125Hz$ and (c) relaxation time τ_α as function of strain λ. In black, the reference curves.

dynamics goes on accelerating after yield and is the fastest at the end of the stress softening regime, where the stress reaches a minimum value. Upon applying further strain, the dominant relaxation time starts to increase at the onset of the SH regime. It increases by roughly a factor 10 between $\lambda = 1.15$ and $\lambda = 1.8$ from about 30 s to about 300 s at $\dot{\lambda} = 2.5 \times 10^{-4} s^{-1}$ and from about 3 s to 30 s at $\dot{\lambda} = 2.5 \times 10^{-3} s^{-1}$. The strain hardening is thus associated with an increase of the dominant relaxation time. Note that in any case, the increase of relaxation times during SH remains moderate, here about 30 s. Even in the strain hardening regime the glassy polymer remains in an strongly accelerated state as compared to the initial one for which the relaxation time after ageing was 10^6 s or more. The evolution of the stretching parameter β in figure 4 is also non-monotonic. β increases first from the intial value between 0.2 and 0.3 to reach a maximum in the stress softening regime ($\beta \approx 0.5$) and then decreases during the strain hardening regime down to approximately 0.4 for $\lambda \approx 1.7$.

According to Chen and Schweizer and to Dequidt *et al* [42, 43], the α-relaxation is an activated process controlled by the presence of free energy barriers. The application of a stress leads to a lowering of these free energy barriers. This point of view accounts for the acceleration of the dynamics upon applying a deformation, from the onset of the non-linear regime before yield up to the stress softening regime. From the increase of the relaxation time τ_α during the strain hardening regime,

and by keeping the picture of the α-relaxation as an activated process still in the regime of strain hardening -which we will justify later on-, we infer that in this regime there is an additional contribution to the free energy barriers that overcompensates the decrease due to the stress and leads to an increase of the relaxation time : the overall free energy barriers increase in the strain hardening regime. From Figure 3.b one can read that for $\lambda = 1.8$, $\dot{\lambda}\tau_\alpha \approx 0.1$ whereas the corresponding stress is of the order of 70 MPa. As a consequence, the measured evolution of the stress in the strain hardening regime is consistent with the fact that this regime is the consequence of the increase of the monomer relaxation time τ_α. This increase of the relaxation time results in an additional contribution to the flow stress of the order of $\sigma_{hard}(\lambda) = G'_g(\tau_\alpha(\lambda) - \tau_{soft})\dot{\lambda}$ where τ_{soft} is the α-relaxation time at the end of the stress softening regime and G'_g is a high frequency (glassy) shear modulus of order 10^9 Pa. This interpretation is in agreement with the conclusions of Hoy and Robbins who attributed the strain hardening to molecular mechanisms similar to those which control yield stress and flow stress [62], that is α-relaxation process and not *e.g.* entropic elasticity.

The increase of the stretching parameter β during deformation, up to the stress softening regime and before the strain hardening regime, which corresponds to a narrowing of the distribution of relaxation times, is interpreted by Conca *et al* as a consequence of a facilitation mechanism [44, 63]. Note that the generic concept of *facilitation*, i.e. the idea that local mobility may be accelerated by a faster environment, is not recent [64, 65]. Subunits with intermediate relaxation times relax first as a consequence of the applied stress (the fast ones relax anyway, disregarding of the applied strain) and acquire a faster dynamical state [43]. Just after yield, some very slow subunits may persist with long relaxation times because they are the longest lived subunits and also because they are no longer submitted to a high level of stress since their neighbors have relaxed [43]. This is especially the case during the stress-softening regime. Without any additional mechanism, these very slow subunits would not relax and should remain long-lived. This situation would result in a broadening of the distribution of relaxation times [43]. However, the very slow subunits are now surrounded by very fast ones. As a consequence, the slow subunits melt by a diffusion process [44] as it is described in Fig.11. This melting process of slow subunits by fast neighboring ones is the facilitation process [23, 24, 63].

The dominant scale for the α-relaxation process is also set by the facilitation mechanism: Merabia and Long proposed that slow dynamics correspond to upwards density fluctuations, and fast domains to downwards density fluctuations [23, 24]. The smaller the scale the larger the flucuations. One may then find denser domains at smaller scales. On the other hand, density fluctuations at very small scale are short-lived as a consequence of their fast surrounding and their small scale. At an intermediate scale ξ, it is possible to have relatively large density fluctuations which are long-lived. This is illustrated in Fig.11 (right). The lifetime of slow domains corresponds to the diffusion time of fast dynamics from their neighbours. As a consequence of the facilitation mechanism, the size $\xi = aN_c^{1/3}$ also sets the effective width of the relaxation time distribution, between τ_α (the long time cut-off) and a short time limit τ_f, according to $\tau_\alpha = N_c^{2/3}\tau_f$. This description, which allows for a calculation of the dominant scale N_c, was found to be of order 1000 monomers, or equivalently $\xi \simeq 3-5$ nm [23], in agreement with NMR experimental results [18]. The temporal asymmetry of the rejuvenation and ageing dynamics in glassy polymers [60] is a direct manifestation of the facilitation mechanism introduced by Merabia and Long [24, 66], which has been confirmed by Medvedev and Caruthers [67].

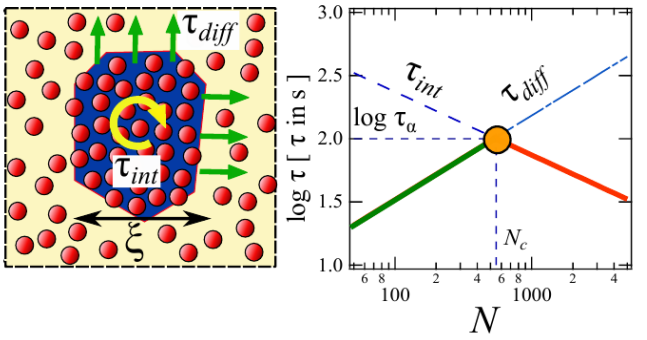

FIG. 11. Left: A slow (high density) subunit of size $\xi \sim 3-5$ nm within a faster (lower density) surrounding may relax either by internal free volume reorganization (time τ_{int}) or diffusion (time τ_{diff}) (density differences are exagerated). Right: variation of $\tau_{int} \sim N^{-1/2}$ (dashed curve) and $\tau_{diff} \sim N^{2/3}$ (dash-dotted curve) vs the number N of monomers in subunits.

The subsequent evolution of the stress after complex histories of deformations such as that of the relaxation protocol or of the unloading protcol has been the object of many studies. The first striking observation (see figures 5 and 8) is that the stress-strain curve rejoins the reference curve after a few tens of percent of subsequent deformation. This behavior is part of what is generically called Bauschinger effect [12, 68]. It means in particular that the relaxations, which take place in the sample during the ageing step do not erase the memory of the first deformation amplitude λ at which the deformation is stopped allowing the ageing of the system. As a consequence, the possible structural evolution responsible for strain hardening appears not to relax, or to relax very slowly and negligibly during ageing at intermediate deformations. These possible structural changes may be chains orientation as hypothesized by Hoy and Robbins [62] or by Chen and Schweizer [34] and measured experimentally by Vogt *et al* [69]. Indeed, chain orientation, which increases

upon the applied deformation, relaxes slowly when the applied stress is removed as compared to the stress which may be suppressed almost instantaneously. Thus, the contribution of the orientation to the free energy barriers $\kappa(\lambda)$ remains constant and positive, whereas the negative contribution of the stress to the free energy barriers cancels almost instantaneously when the macrocospic stress is suppressed as we will discuss below.

On the other hand, we do observe for protocol II an overshoot of the stress that is present upon resuming the deformation, followed by a stress softening regime. Qualitatively at least, the first 10-15% of subsequent deformation after the ageing step are similar to the first deformation at the beginning of the experiment, though the initial slope is steeper for the second deformation as compared to the first one. This feature is classically observed when studying Bauschinger effect [12, 68, 70]. We deduce from this observation that the degrees of freedom which set the free energy barriers for α-relaxation corresponding to yield and stress softening have relaxed. This is a well-known feature. At short times after a first large amplitude deformation, the overshoot of the stress and the stress-softening regime are suppressed [3, 71]. This overshoot and the ensuing stress softening regime appear again after a relatively short time scale allowed for ageing as characterized by Govaert *et al* [3, 6, 72]. From these classical observations, we deduce that the degrees of freedom which control the free energy barriers associated to yield and stress softening are different from those which control the free energy barriers associated to strain hardening. The first ones relax relatively fast, on time scales of a few thousand of seconds as studied by Govaert *et al* by an ageing process, whereas the second do not relax on times scales of a few hours or even tens of hours.

From this discussion, we deduce that the effect of the applied deformation on the free energy barriers for α-relaxation is the sum of two contributions: 1) a contribution due to the stress, which reduces the free energy barriers; 2) a contribution of chains orientation, which increases the free energy barriers. These two contributions are discussed in the next subsection.

IV.2. Free energy barriers dependence on the stress and on chain orientation

α-relaxation is an activated process. In the presence of a local stress σ, and before strain hardening takes place, Dequidt *et al* [43] and Conca *et al* [44] have proposed recently that the free energy barrier for α-relaxation is given by

$$\Delta F(\sigma, T, \rho) = \Delta F_0(T, \rho) - \frac{\xi^3 \sigma : \sigma}{2G'_g} \qquad (2)$$

$\xi \sim N_c^{1/3} a \sim 5$nm is the characteristic length of dynamical heterogeneities where α-relaxation takes place. $a \sim 0.5$ nm is a monomer size. $\Delta F_0(T, \rho)$ is the free energy barrier for the polymer at rest before stress has been applied. It depends on the temperature, on the local state (density ρ), and on the ageing process undergone by the considered sub-units. The quantity $\sigma{:}\sigma$ is the invariant defined as $\sigma{:}\sigma = (1/2)\left[(\sigma_1-\sigma_2)^2+(\sigma_2-\sigma_3)^2+(\sigma_3-\sigma_1)^2\right]$ where $\sigma_1, \sigma_2, \sigma_3$ are the eigenvalues of σ, the local stress tensor. In pure shear deformation it is equal to $3\sigma_{xy}^2$ where σ_{xy} is the stress component associated with the y and x-axes.

One sees that the stress lowers the free energy barriers quadratically. For a glassy polymer which has aged for 6 months and which has a relaxation time of the order of 10^6 s, this barrier is of the order of $\tau_0 \exp(\frac{\Delta F_0}{k_B T}) \sim 10^6$s, where $\tau_0 \sim 10^{-12}$s is a balistic time between collisions on the monomer scale and k_B is the Boltzmann constant. The barrier is thus of the order of $\Delta F_0 \approx 45 k_B T$. Under an applied stress σ, the corresponding relaxation time τ is given by :

$$\tau_\alpha(T, \rho, \sigma) = \tau_\alpha(T, \rho) \exp\left(-\frac{\xi^3}{2\, k_B T}\, \frac{\sigma : \sigma}{G'_g}\right) \qquad (3)$$

Note that Equation 3 incorporates explicitly only the effect of the deviatoric stress and not the effect of the hydrostatic component of the stress. Taking the deviatoric stress into account is sufficient when considering only either tensile test experiments or deformation in compression [45, 46, 68, 73], because the effect of the hydrostatic component on the relaxation time is relatively small as compared to that of pure shear. On the other hand one must take this effect into account when one aims at comparing tensile test experiments with those in in compression [13, 48]. This is done by adding a multiplicative factor on the r.h.s of Equation 3 of the type $\exp(p/p_0)$ where p is the hydrostatic component of the stress and p_0 is a constant of the order of 10^8 Pa typically. For the considered experiments, the argument p/p_0 never exceeds the value of the order of 1, whereas the relaxation times vary by many orders of magnitude due to the deviatoric component [48].

It is important to note that the change of free energy barriers *per monomer* due to the stored elastic energy, at yield, as compared to the thermal energy $k_B T$, $\delta f / k_B T = a^3 \sigma : \sigma / (2 k_B T G'_g)$ is very small, of the order of 10^{-2}. At the scale of N_c monomers (or equivalently at the scale ξ^3), the decrease of free energy barrier $N_c \delta f / k_B T = \xi^3 \sigma : \sigma / (2 k_B T G'_g)$ is of the order of 10. When the applied stress reaches the value $\sigma_y \sim$ *e.g.* 70 MPa, it follows that the free energy barrier for relaxation drops from *e.g.* $45 k_B T$ to $35 k_B T$, which corresponds roughly to $\tau_\alpha \sim 10^4$s, that is the time scale of the experiment [45]. Note that these estimates are comparable to those of Hebert *et al* [55] and of Bennin

et al [30] who discussed the activated nature of the α-relaxation process during plastic flow.

Even though the stress increases during the course of deformation in the strain-hardening regime, the relaxation time increases as well. As a consequence, we expect that the free energy barriers increase as compared to Equation (2). Given Equation (2) and its proposed extension for taking SH into account, the free energy barrier per monomer should be given by an expression of the type :

$$\delta f(\sigma, \lambda) = \delta F_0 - \frac{a^3 \sigma : \sigma}{2G_0'} + \kappa(\lambda) \tag{4}$$

where $\kappa(\lambda)$ is the positive contribution to the free energy barrier per monomer of the microscopic mechanism responsible for strain hardening which overcompensates the decrease of the free energy barrier due to the stress. δF_0 is the free energy barrier per monomer in the glassy state, typically $4 \times 10^{-2} k_B T$. An increase of the relaxation time τ_α by about one decade (slightly less more precisely) between stress softening and a deformation amplitude of $\lambda = 1.7$ corresponds to an overall increase of the free energy barriers per monomer of order $0.005 k_B T$. Since the contribution of the stress to the reduction of the free energy barriers between stress softening and the deformation $\lambda = 1.7$ is of the order of $0.005 k_B T$, we deduce that the contribution of the mechanim which leads to stress hardening, $\kappa(\lambda = 1.7)$, is of the order of $0.01 k_B T$ per monomer, that is of the order of 10 $k_B T$ on the scale N_c of dynamical heterogeneities. During these various regimes, the α-relaxation process remains an activated process, with barriers larger than $35 - 40 k_B T$.

The scale $\xi \sim 5$ nm or $N_c \sim 1000$ plays a key role for plastic deformation. Its temperature dependance has been deduced from small probe diffusion measurements [17]. To this date, no experiment hints to a stress dependence of ξ. Note that Ediger experiments in reference [28] could be accounted for a single ξ value at different stress level. At this stage we will consider that ξ is constant during applied deformation, though such an assumption warrants further experimental investigations.

Recent work performed by molecular dynamics simulations relate also chain orientation with strain hardening behavior [62]. It is important to note that chain orientation does not intervene in strain hardening through chain elasticity as described by Haward [8] but through enthalpic effects of the same nature that control yield and flow stress, that is free energy barriers on the monomer level associated to α-relaxation. The term $\kappa(\lambda)$ in Equation (4) is the contribution of the structural change to the free energy barrier for α-relaxation. We deduce from our experiments, as well as classical results regarding strain hardening that this contribution relaxes slowly *e.g.* once the applied strain is stopped. As a consequence, we propose that a future theory aimed at describing the physics of strain hardening should propose a dynamical description of chain orientation under applied deformation taking into account the local relaxation time and the heterogeneous nature of the dynamics. Conca [74] proposed such an equation for monomer orientation resulting from the competition between applied strain which induces stretching of the monomers, and entropic relaxation of the orientation on the monomer scale. Note that Hoy and O'Hern introduced such an equation on a larger scale corresponding to the overall chains [75].

On the other hand according to Equations (2) and (3), the stress contribution to the free energy barriers relaxes immediately when the stress is brought back to zero. In the expression regarding the change of free energy per monomer due to the stress σ and to chains orientation (Equation (4)), the contribution due to the stress adjusts instantaneoulsly to the applied stress (apart from stress fuctuations on the local scale due to disorder), whereas $\kappa(\lambda)$ relaxes very slowly and may require days or weeks or more to relax. The effects of stress and of chain orientation behave very differently as regards to their contribution to free energy barriers. This is observed in fig.5(d) and fig.10(c), where we see that the dominant relaxation time increases rapidly during the ageing step when $\dot{\lambda} = 0$. On the contrary, the dominant relaxation time drops rapidly upon resuming the deformation as can be observed in the same figures, or also at the very beginning of the applied deformation. The effect of the stress on the relaxation times is very fast as it is implied by Equation (3). The key for describing strain hardening of glassy polymers is the quantitative description of chain orientation dynamics as we have just discussed.

In Figure 4.(b) we observe that the stretching parameter β decreases with τ_α for stretched samples: at high strain rates, the distribution of relaxation times gets narrower. This effect has also been observed in PMMA by Ediger and collaborators in several experiments [26, 27]. Here, β varies between 0.5 and 0.38 which are values larger than typical β values of polymers at rest, which can be as low as $0.2 - 03$ [26, 27]. There is not yet a complete understanding for the master curve of Figure 4.(b), but we may undertsand why the distribution gets narrower under stress as compared to the polymer at rest. This effect is the results of two mechanisms: the first one is the acceleration of the dynamics by the stress as discussed with equation (2): slower subunits support larger stress as compared to faster ones before relaxing. As a consequence, the fact that they are more accelerated contributes to make the RTD narrower. The second mechanism which contributes to this effect is the facilitation mechanism: some slow subunits may persist with a very low stress applied onto them when their neighbors have all relaxed. This would contribute to a broadening of the relaxation time distribution. On the other hand, these slow subunits relax and become faster ones as a

consequence of the facilitation mechanism which melts them [24, 44].

Without explicitly describing a coupling between chain orientation and the α-relaxation time, Hoy and O'Hern [75] introduced a coupling between chain orientation and the ability of the polymer glass to build an increasing stress during applied deformation. For this purpose, they introduced a dynamical equation in order to calculate large scale chain orientation evolution during applied strain. Large scale chain orientation relaxes slowly, with relaxation time scaling as the molecular weight N of the chains during applied strain, and as N^2 upon cessation of the flow. In the picture of Hoy and O'Hern, the stress increase is a direct effect of chain orientation and the associated increase in size of plastic events correlation zone. Memory effects are incoporated in the model as a consequence of the slow relaxation of large scale chain orientation. Their approach may then also be tested to interpret the kind of effects that we discuss in this article.

IV.3. Interpreting the memory effects

The stress-strain curve of the relaxation protocol (Figures 7(a) and 7(d)), together with Figures 7(b) and 7(e) may give some indications regarding the relaxation processes at play during plastic flow. We have just discussed that the yield behavior is associated to a contribution which lowers the free energy barriers, the stored elastic energy on scale ξ according to Dequidt *et al* [43]. This contribution relaxes partially during the relaxation protocol, otherwise the second deformation would recover the reference curve immediately, but this relaxation is not complete, otherwise the second deformation should superimpose (if shifted adequately) to the reference curve. Here also, we deduce that the internal variables that control the first part of the deformation curve, up to yield and strain softening, relax relatively fast, in particular when the applied stress is non zero as it has been shown by Clarijs *et al* [72]. On the other hand, the fact that the stress-strain curve and the $\tan\delta$ curve come back on the reference curve after 20% of deformation indicates that the internal variables that control the stress-hardening process relax more slowly. This is consistent with our proposition that the free energy barriers variations during applied strain is the sum of two different contributions: one which is a function of the stress and another one which is a function of chain orientation. The first contribution evolves rapidly, *e.g.* when the stress is relaxed, the second one is a slow variable, which requires chain conformation relaxation.

After resuming the deformation, two opposite effects are at work regarding the evolution of the free energy barriers for α-relaxation and therefore for the evolution of the α-relaxation time and the whole distribution of relaxation times. First, the stress increases, which contributes to decreasing the free energy barriers according to Equations (3)-(2) and therefore to the acceleration of the dynamics and to the rise of $\tan\delta$. In the same time, the structural change in the sample, that is the chains orientation, which contributes to increasing the free energy barriers goes on. Upon resuming the deformation, chains orientation starts increasing again. This structural change does not start from zero because chain orientation is slow to relax and has negligibly relaxed during the waiting time. This contribution tends to increase the free energy barriers, therefore to increase the relaxation times and thus to reduce the increase of $\tan\delta$ as compared to the first deformation from the inital system. The applied deformation has simultaneously these two effects. The effect of the strain hardening mechanism is apparent on the aged systems because the acceleration of the dynamics requires about 10% of deformation, similarly to the reference curve in its initial state. On the other hand, during these additional 10% deformation, the structural change is enhanced and the free energy barriers for relaxation increase due to the initial non zero contribution which is absent for the undeformed reference system. The smaller value reached by $\tan\delta$ upon resuming deformation, and the broadening of its evolution to rejoin the reference curve are the consequences of the contribution of chains orientation to the free energy barriers. This effect can be observed in Figure 5(d) where we plot the evolution of τ_α during the course of the second protocol. One can observe that τ_α decreases rapidly after resuming the deformation at time $t = 5000$ s. τ_α reaches a minimum which corresponds to a larger value as compared to the initial deformation: about 100 s instead of 30 s. The larger minimum value of τ_α is the consequence of the long-lived increase of free energy barriers associated to the strain hardening mechanism.

IV.4. Comparison between relaxation protocol and unloading protocol

It can be observed that both the dielectric response and the mechanical response differ strongly between protocol II and III. The first specific difference between these two protocols is the appearence of a stronger stress overshoot in the relaxation protocol as compared to the unloading protocol, and a broader dielectric response in protocol II as compared to protocol III.

This effect may be understood as a consequence of stress-accelerated ageing [72]. It has been observed long ago by Vincent [56] and other groups [13] that ageing is faster in a glassy polymer under an intermediate level of applied stress as compared to a totally unloaded polymer. In protocol III, the stress is completely removed during the ageing step. As a consequence, the relaxation times associated to ageing dynamics increase very rapidly as observed in Figure 10c. This is consistent with Equation (2): the state of the sample does not evolve in a measurable way during the ageing step. This

suppression of ageing is thus responsible for the almost immediate recovery of the reference stress-strain curve. From the fact that the same observation can be made for the dielectric response (Figure 10.b), which recovers the reference curve immediately after resuming the deformation, one can infer that the whole spectrum of relaxation times is practically frozen during the ageing step of protocol III.

Merabia and Long have described the structural relaxation of a glassy polymer upon heating or upon cooling [24]. They introduced a stochastic model for describing the evolution of the distribution of density ρ and of the ensuing distribution of $\tau(T,\rho)$ under any temperture history. It allowed us to describe *e.g.* how the system evolves towards higher density after a temperature down jump. The dynamics of structural evolution towards higher densities after quenching, or lower densities after heating, is described by a Fokker-Planck equation in density space. The kinetics coefficient of this equation read $\gamma(\rho) \sim \tau^{-1}(\rho,T)$ which are diffusion coefficient in density space. The value assumed by $\gamma(\rho)$ depends not only on ρ but on the whole density distribution $p(\rho)$ through the facilitation mechanism. This equation describes the structural relaxation of the polymer samples towards the equilibrium distribution of density $p_{eq}(\rho,T)$. In the absence of applied stress, $\tau(\rho,T)$ is given by the WLF law expressed as a function of the density at a given temperature. Under a shallow temperature down jump, the distribution of the density fluctuations evolves towards larger densities, and the corresponding distribution of relaxation times towards longer relaxation times as described in Figure 12. On the other hand, if the temperature is too low, as it is the case for polycarbonate at room temperature, this ageing does not take place because the relaxation times $\tau(\rho,T)$ become too long.

Dequidt *et al* and Conca *et al* [43, 44] considered how the distribution of relaxation times evolves under applied strain or stress. Equation (3) expresses the fact that in the presence of a deviatoric stress $\sigma - 1/3Tr(\sigma)I_d$, the dynamics is accelerated. The decrease of the α-relaxation time may allow the sample to flow (plastic flow). It may also allow the system to age structurally according to the Fokker-Planck equation of reference [24] since these are the same α-relaxation processes which are involved in flow or for densification of the sample [39]. This densification leads to an increase of the first term $\tau(T,\rho)$ on the r.h.s of equation (3). The progressive increase of the corresponding distribution of relaxation times is responsible for the stress overshoot and stress softening in the second protocol as well as the overshoot of $\tan\delta$ and the slow recovery of the $\tan\delta$ curve on the reference curve. If one assumes that the stress is uniform, studying structural ageing under applied stress thanks to the Merabia-Long Fokker-Planck equation amounts just to rescale the time scale by the factor $\exp\left(-\frac{\xi^3}{2T}\frac{\sigma:\sigma}{G_0'}\right)$. On the other hand, regarding the third protocol, the stress in the r.h.s. of equation (3) (which is not strictly zero due to fluctuations in a disordered sample) is much smaller than for the second protocol. The distribution of relaxations times $(\tau(T,\rho,\sigma))$ is shifted to larger values and no structural ageing is possible. The densification of the material cannot take place. There is thus no stress overshoot and no stress softening upon resuming the deformation. The ensuing response of the system rejoins almost immediately the curve of the reference protocol as can be observed for both the mechanical and the dielectric response.

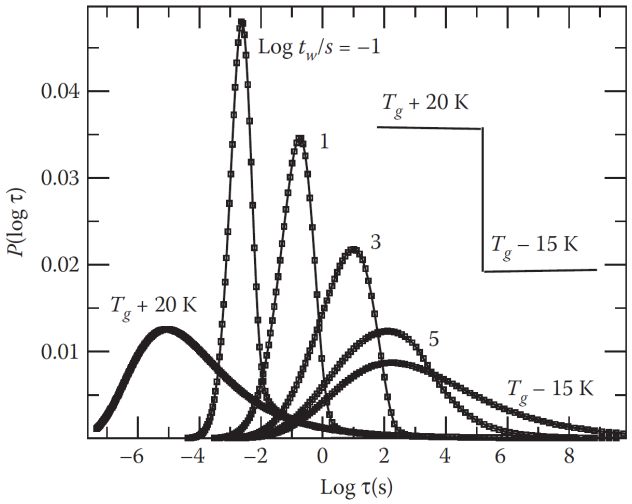

FIG. 12. Ageing dynamics of a polymer after a shallow temperature down jumps. One plots here the evolution of the distribution of relaxation times after a waiting time up to 10^5 s. In the case of a down jump to a much lower temperature, and in the absence of stress, this dynamics is frozen, whereas the imposition of an intermediate level of stress may allow ageing to take place. The underlying ageing mechanism is associated to a progressive evolution of the density distribution towards larger densities [24]

V. DISCUSSION AND CONCLUSION

Among the earliest experiments aiming at studying how a predeformation modifies the relaxation times spectrum, researchers performed mechanical spectroscopy experiments (see *e.g.* reference [76] and references therein). The authors applied to the samples a first deformation, and then small oscillatory perturbations for measuring the viscoelastic response in this transient state. Belguise *et al* [46] performed recently experiments in the same spirit with a precision far beyond those previously achieved. They measured the subsequent stress relaxation functions. The spectrum of these relaxation functions could be quantitatively fitted by using the model of Long *et al* [39, 43, 45]. They confirmed quantitatively that the free energy barriers are reduced by an amount quadratic in the applied stress, that is the stored elastic

energy on the scale ξ of the α-process, and that this scale is of the order of 5-6 nm [46].

Upon deformation, up to the onset of the strain hardening regime, we observe that the width of the distribution of relaxations time decreases, which is quantified by the evolution of the stretching parameter β. This effect can be understood as a consequence of the facilitation mechanism which is at the very heart of the α-relaxation process [23, 24, 45]. We proposed that the change of free energy barriers due to the applied strain is the sum of two terms: 1) one which is a function of the local stress. 2) a second one which is a function of the local monomer orientation. The first one relaxes immediately as a function of the applied stress whereas the second one relaxes very slowly deep in the glassy state. The slow relaxation of chains orientation could explain the various memory effects observed in the strain hardening regime and generically named Bauschinger effect. It could explain the fact that a second deformation after some waiting time at some point in the strain hardening regime rejoins the reference curve, whereas a yield stress is present for this second deformation: the degrees of freedom which control the free energy barriers associated to yield relax fast, whereas the degrees of freedom which control the free energy barriers associated to plastic flow in the strain hardening regime (monomers orientation) relax slowly. This mechanism could also explain both the dielectric response during the second protocol, and the mechanical response, and various features such as the relative values of the $\tan\delta$ peaks in the first deformation and that during the second deformation, as well as the delay before the second curve rejoins the reference one. We propose that the broadening of the distribution of relaxation times in the strain hardening regime is the consequence of this increase of free energy barriers. Indeed, the latter slows down all the subunits and makes the facilitation process less and less efficient. Note that theoretical calculations have shown that without facilitation process, the distribution of relaxation times should broaden under applied strain, even without strain hardening mechanism [43, 44].

Ediger and co-workers performed similar measurements [26–28] by studying the reorientation dynamics and by performing successive steps of deformation. They performed creep experiments at constant engineering stress. At various steps, they removed the stress altogether and waited for different periods of time before resuming the creep experiment. Among the various features observed in their experiments, they measured the evolution of the relaxation time after the stress is completely suppressed at some point in the SH regime. A drop of the dominant relaxation time by almost two decades is observed (see Figure 5.(b) in reference [27]). After this drop, shortly after stress removal, the relaxation time increases again during the ensuing ageing process. Simultaneously, just after the stress is suppressed, a contraction of the sample is observed by a large amount, close to 10%. A large part of this contraction is fast as compared to the time resolution of the experiment.Then, the relaxation of the sample deformation goes slowly at longer time scales. This specific feature of the memory effects studied by the group of Ediger can be understood qualitatively by the mechanisms that we introduced in this manuscript: during the retraction step, the orientation of the monomers decreases rapidly. This results in a decrease of the free energy barriers. As it happens, this decrease of the free energy barriers is larger than the increase due to stress removal: the overall evolution of the free energy barriers is negative and the relaxation time decreases. Subsequently, the sample starts ageing and the relaxation time increases again.

On the modelling and or theoretical side, plastic deformation of polymers has been considered by Schweizer and co-workers within the NLE model [34, 41, 63]. The Schweizer model allows for describing the stress softening effect, a defining feature of aged glassy polymers, whereas some other models do not [77, 78]. Note that the decrease of the free energy barriers as a function of the applied stress in the theory of Schweizer *et al* [41] is a convex function with a non-zero slope at $\sigma = 0$. It is thus qualitatively different from the quadratic function $-\sigma : \sigma$ introduced by Dequidt *et al* [39, 43] which is concave and has a slope zero at $\sigma = 0$. Note also that according to the theory of Schweizer *et al*, the barrier cancels altogether at a critical value of the stress σ_c, whereas in the theory of Dequidt *et al* barriers are present at any value of the stress: the flow remains activated with free energy barriers of the order of 30-35 k_BT at least. A fundamental difference also between these two approaches is the scale involved in the α-relaxation process: Dequidt *et al* assume that this scale involves about $N_c \sim 1000$ of monomers [23, 43] whereas Schweizer *et al* consider cages of order 10 monomers [41]. Medvedev and Caruthers [77] have adapted the stochastic model introduced by Merabia and Long [24] to study the evolution of the distribution of relaxation times under an applied stress instead of a temperature change. They introduced a coupling between the stress and the free energy barrier $\Delta F \propto (\sigma_c^2/\sigma^2 - 1)$ which is also very different from the coupling introduced by Dequidt *et al* [39, 43] and is also a convex function instead of a concave one, with a non zero slope at small stress. It is very different from the coupling obtained for interpreting their experimental data in reference [46].

Strain hardening *per se* has been recently studied by Zou *et al*, by coarse-grained molecular dynamics simulations [79, 80]. In their simulations they renounce to describe yield and plastic flow itself. The latter is introduced phenomenologically in a one parameter model. In this picture, coarse-grained polymer beads interact

with an abstract glassy sea in which they are embedded. They are dragged by the applied deformation and strain hardening results from the strong elongation of chain segments forming hair-pins and of finite extensibility and of strongly non-linear tension as a function of their extension. The friction parameter is an unwarranted adjustable parameter which allows the formation of the strain hardening due to the springs extension produced by the applied strain. Indeed these springs do not have the time to relax due to the high friction within the abstract glassy background. Note that the model of Zou *et al* is not able to obtain the experimentally observed strain hardening in shear. Furthermore it does not predict changes in the relaxation times. Our and other experiments show that these changes, which are not monotonic as a function of the applied stress, are key features of plastic deformation and of strain hardening in stretched glassy polymers [26, 27, 33, 37].

In conclusion, we have studied the evolution of the dominant relaxation time and of the relaxation times distribution, when the sample is deformed from the linear regime to the strain hardening regime up to very large strain. We have also considered complex protocols during which the deformation is first stopped at intermediate values of the strain and then resumed after different waiting times. There is currently no theory for calculating the evolution of the distribution of relaxation times in the strain hardening regime but our experimental results point towards an increase of the free energy barriers due to chain orientation in this regime, consistently with the model proposed by Chen and Schweizer [34]. This chain orientation contribution to the free energy barriers relaxes very slowly whereas the contribution of the stress as described in references [43–45] evolves almost immediately with the applied stress. Our experiments and the associated discussions provide routes for a spatial calculation of the evolution of the distribution of relaxation times up the strain hardening regime. We propose that, in order for quantitatively explaining our resuts as well as other results from the literature, theoretical and experimental works should aim, in particular, at describing the evolution of the monomer orientation distribution as a function of the thermo-mechanical history of the samples. Finally, let us note that we have studied aged samples for which we do not know the exact ageing histories. Senden et al [81] have studied various ageing conditions on PC. Though these conditions have an impact on stress-softening, they found that the strain hardening regime was essentially unsensitive to these various ageing histories. We expect then our results to be robust at this regard. On the other hand, performing similar experiments as ours on samples undergoing various ageing histories should be of high interest for a deeper understanding of the various relaxation mechanisms.

ACKNOWLEDGMENTS

J. Hem acknowledges the funding by Solvay. We thank O.Razebassia, A. Petrosyan and the Bartolo team for helpful assistance on the tensile machine and the preparation of samples.

[1] J. D. Ferry. *Viscoelastic Properties of Polymers*. John Wiley and Sons, Inc., 1980.

[2] L. E. Nielsen and R. F. Landel. *Mechanical Properties of Polymers and Composites*. Marcel Dekker, New York, 1994.

[3] H.E.H. Meijer and L.E. Govaert. Multi-scale analysis of mechanical properties of amorphous polymer systems. *Macromolecular Chemistry and Physics*, 204(2):274–288, 2003.

[4] R.N. Haward. *The Physics of Glassy Polymers*. Applied Science Publishers, London, 1973.

[5] H. E. H. Meijer and L. E. Govaert. Mechanical performance of polymer systems: The relation between structure and properties. *Prog. Polym. Sci.*, 30:915–938, 2005.

[6] H.G.H Van Melick, H.E.H. Meijer, and L.E. Govaert. On the origin of strain hardening in glassy polymers. *Polymer*, 44:2493–2502, 2003.

[7] J. Richeton, S. Ahzi, L. Daridon, and Y. RÃ©mond. A formulation of the cooperative model for the yield stress of amorphous polymers for a wide range of strain rates and temperatures. *Polymer*, 46:6035–6043, 2005.

[8] R.N. Haward. Strain hardening of thermoplastics. *Macromolecules*, 26:5860–5869, 1993.

[9] E.J. Kramer. Open questions in the physics of deformation of polymer glasses. *Journal of polymer science. Part B. Polymer physics*, 43:3369–3371, 2005.

[10] M. C. Arruda, E. M.; Boyce. Evolution of plastic anisotropy in amorphous polymers during finite straining. *International Journal of Plasticity*, 9:697–720, 1993.

[11] R.N. Haward. Effects of initial anisotropy on the finite strain deformation behavior of glassy polymers. *International Journal of Plasticity*, 9:783–811, 1993.

[12] D.J.A. Senden, J.A.W. van Dommelen, and L.E. Govaert. Strain hardening and its relation to bauschinger effects in oriented polymers. *Journal of Polymer Science Part B: Polymer Physics*, 48:1483–1494, 2010.

[13] E. T. J. Klompen, T. A. P. Engels, L. E. Govaert, and H. E. H. Meijer. Modeling of the postyield response of glassy polymers: Influence of thermomechanical history. *Macromolecules*, 38:6997–7008, 2005.

[14] A. Charvet, C. Vergelati, P. Sotta, and D. R. Long. Damage mechanisms of plasticized cellulose acetate under tensile deformation studied by ultrasmall-angle x-ray scattering. *Macromolecules*, 52:6613â€“6632, 2019.

[15] S. Djukic, A. Bocahut, J. Bikard, and D. R. Long. Study of damage mechanisms of amorphous and low semicrystalline polymers under tensile deformation by ultrasmall-angle x-ray scattering. *Macromolecules*, 53:5538–5529, 2020.

[16] M. D. Ediger, C. A. Angell, and S. R. Nagel. Supercooled liquids and glasses. *J. Phys. Chem*, 100:13200–13212, 1996.

[17] M.D. Ediger. Spatially heterogeneous dynamics in supercooled liquids. *Annu. Rev. Chem.*, 51:99–128, 2000.

[18] U. Tracht, M. Wilhelm, A. Heuer, H. Feng, K. Schmidt-Rohr, and H.W. Spiess. Length scale of dynamic heterogeneities at the glass transition determined by multidimensional nuclear magnetic resonance. *Phys. Rev. Lett.*, 81:2727 – 2730, 1998.

[19] M. T. Cicerone, F. R. Blackburn, and M. D. Ediger. Anomalous diffusion of probe molecules in polystyrene - evidence for spatially heterogeneous segmental dynamics. *Macromolecules*, 28:8224 – 8232, 1995.

[20] L. Berthier, G. Biroli, J.-P. Bouchaud, L. Cipelletti, D. El Masri, D. L'HÃ´te, F. Ladieu, and M. Pierno. Direct experimental evidence of a growing length scale accompanying the glass transition. *Science*, 310(5755):1797–1800, 2005.

[21] C. Crauste-Thibierge, C. Brun, F. Ladieu, D. L'Hôte, G. Biroli, and J-P. Bouchaud. Evidence of growing spatial correlations at the glass transition from nonlinear response experiments. *Phys. Rev. Lett.*, 104:165703, Apr 2010.

[22] S. Albert, Th. Bauer, M. Michl, G. Biroli, J.-P. Bouchaud, A. Loidl, P. Lunkenheimer, R. Tourbot, C. Wiertel-Gasquet, and F. Ladieu. Fifth-order susceptibility unveils growth of thermodynamic amorphous order in glass-formers. *Science*, 352(6291):1308–1311, 2016.

[23] S. Merabia and D. Long. Heterogeneous dynamics in van der waals liquids. determination of the characteristic scale. *Eur. Phys. J. E*, (9):195–207, 2002.

[24] S. Merabia and D. Long. Heterogeneous dynamics, ageing, and rejuvenating in van der waals liquids. *J. Chem. Phys.*, 125(23):234901, 2006.

[25] L. S. Loo, R. E. Cohen, and K. K. Gleason. Chain mobility in the amorphous region of nylon 6 observed under active uniaxial deformation. *Science*, 288:116–119, 2000.

[26] H.-N. Lee, K. Paeng, S. F. Swallen, and M. D. Ediger. Direct measurement of molecular mobility in actively deformed polymer glasses. *Science*, 323:231–234, 2009.

[27] H.-N. Lee, R. A. Riggleman, J. J. de Pablo, and M. D. Ediger. Deformation-induced mobility in polymer glasses during multistep creep experiments and simulations. *Macromolecules*, 42(12):4328–4336, JUN 23 2009.

[28] H.-N Lee, K. Paeng, S.F. Swallen, M.D. Ediger, R.A. Stamm, G.A. Medvedev, and J.M. Caruthers. Molecular mobility of poly(methyl methacrylate) glass during uniaxial tensile creep deformation. *J. Polym. Sci.: Polym. Phys. Ed.*, 47:1713–1727, 2009.

[29] K. Hebert and M.D. Ediger. Reversing strain deformation probes mechanisms for enhanced segmental mobility of polymer glasses. *Macromolecules*, 50:1016–1026, 2017.

[30] T. Bennin, J. Ricci, and M.D. Ediger. Enhanced segmental dynamics of poly(lactic acid) glasses during constant strain rate deformation. *Macromolecules 2020*, 52:6428–6437, 2019.

[31] J. Kalfus, A. Detwiler, and A. J Lesser. Probing segmental dynamics of polymer glasses during tensile deformation with dielectric spectroscopy. *Macromolecules*, 45: 4839–4847, 2012.

[32] R. Perez-Aparicio, D. Cottinet, C. Crauste-Thibierge, L. Vanel, P. Sotta, J.-Y. Delannoy, D. R Long, and S. Ciliberto. Dielectric spectroscopy of a stretched polymer glass: heterogeneous dynamics and plasticity. *Macromolecules*, 49(10):3889–3898, 2016.

[33] R. Sahli, J. Hem, C. Crauste-Thibierge, F. Clement, D. R. Long, and S. Ciliberto. Relaxation time of a polymer glass stretched at very large strains. *Phys. Rev. Mater.*, 4(3), 2020.

[34] K. Chen and K. S. Schweizer. Suppressed segmental relaxation as the origin of strain hardening in polymer glasses. *Phys. Rev. Lett.*, 102:038301, 2009.

[35] R. S. Hoy and M. O. Robbins. Strain hardening of polymer glasses: Entanglements, energetics, and plasticity. *Physical Review E*, 77, 2008.

[36] R.; Editor Connie B. Roth Hoy. *Polymer Glasses. Chapter: Modeling strain hardening in polymer glasses using molecular simulations. pp 425-450.* Taylor and Francis Group: Boca Raton, 2016.

[37] J. Hem, C. Crauste-Thibierge, F. Clément, D. R. Long, and S. Ciliberto. Simultaneous memory effects in the stress and in the dielectric susceptibility of a stretched polymer glass. *Phys. Rev. E*, 103:L040502, 2021.

[38] R. S. Hoy and M. O Robbins. Scaling of the strain hardening modulus of glassy polymers with the flow stress. *Polymer Physics*, 47:1406–1411., 2009.

[39] A. Dequidt, D.R. Long, P. Sotta, and O. Sanseau. Mechanical properties of thin confined polymer films close to the glass transition in the linear regime of deformation: Theory and simulations. *Eur. Phys. J. E*, 35:61, 2012.

[40] R. Masurel, S. Cantournet, A. Dequidt, D. Long, H. Montes, and F. Lequeux. Linear viscoelasticity of polymer in their glass transition domains : 2d finite elements simulations. *Macromolecules*, 48:6690–6702, 2015.

[41] K. Chen and K. S. Schweizer. Stress-enhanced mobility and dynamic yielding in polymer glasses. *Europhysics Letters*, 79(2):26006, 2007.

[42] K. Chen and K.S. Schweizer. Theory of yielding, strain softening, and steady plastic flow in polymer glasses under constant strain rate deformation. *Macromolecules*, 44:3988â€“4000, 2011.

[43] A. Dequidt, L. Conca, J.Y. Delannoy, P. Sotta, F. Lequeux, and D.R. Long. Heterogeneous dynamics and polymer plasticity. *Macromolecules*, 49:9148–9162, 2016.

[44] L. Conca, A. Dequidt, P. Sotta, and D. R. Long. Acceleration and homogenization of the dynamics during plastic deformation. *Macromolecules*, 50(23):9456–9472, 2017.

[45] D.R. Long, L. Conca, and P. Sotta. Dynamics in glassy polymers: The eyring model revisited. *Phys. Rev. Mater.*, 2:105601, 2018.

[46] A. Belguise, S. Cantournet, F. Lequeux, and H. Montes. Weak nonlinearities in viscoelastic mechanical properties of polymers near their glass transition: Local versus macroscopic laws for stress-induced acceleration of the mechanical response. *Phys. Rev. M*, 5:33601, 2021.

[47] B. Bending, K. Christison, J. Ricci, and M. D. Ediger. Measurement of segmental mobility during constant strain rate deformation of a poly(methyl methacrylate) glass. *Macromolecules*, 47:800 – 806, 2014.

[48] Th. Merlette. *Theory of strain hardening of glassy polymers.* PhD thesis, Lyon, 2022.

[49] R. Pérez-Aparicio, C. Crauste-Thibierge, D. Cottinet, M. Tanase, P. Metz, L. Bellon, A. Naert, and S. Ciliberto. Simultaneous and accurate measurement of the dielectric constant at many frequencies spanning a wide range. *Rev. Sci. Instrum.*, 86(4):044702, 2015.

[50] H. Watanabe, Y. Matsumiya, and T. Inoue. Rheodielectrics in oligomeric and polymeric fluids: a review

of recent findings. *Journal of Physics: Condensed Matter*, 15:S909–S921, 2003.

[51] P. Lunkenheimer, U. Schneider, R. Brand, and A. Loid. Glassy dynamics. *Contemporary Physics*, 41:15–36, 2000.

[52] F. Kremer and A. Schonhals. *Broadband Dielectric Spectroscopy*. Springer, Berlin, 2003.

[53] B. Bending and M.D. Ediger. Molecular mobility of poly(methyl methacrylate) glass during uniaxial tensile creep deformation. *J. Polym. Sci.: Polym. Phys Ed*, 54: 1957–1967, 2016.

[54] A. F. Yee, R. J. Bankert, K. L. Ngai, and R. W. Rendell. Strain and temperature accelrated relaxation in polycarbonate. *J. Polym. Sci.: Part B: Polym. Phys.*, 26:2463–2483, 1988.

[55] K. Hebert, B. Bending, J. Ricci, and M. D. Ediger. Effect of temperature on postyield segmental dynamics of poly(methyl methacrylate) glasses: Thermally activated transitions are important. *Macromolecules*, 48(18):6736–6744, 2015.

[56] P. I. Vincent. The necking and cold-drawing of rigid plastics. *Adv. Polym. Sci.*, 1:7, 1960.

[57] E. J. Kramer. Stress aging in anhydrous nylon 6?10. *J. Appl. Phys.*, 41:4327, 1970.

[58] C. Dreistadt, A. S. Bonnet, P. Chevrier, and P. Lipinski. Experimental study of the polycarbonate behaviour during complex loadings and comparison with the boyce, parks and argon model predictions. *Materials and Design*, 30:3126–3140, 2009.

[59] M. Doi and S.F. Edwards. *The Theory of Polymer Dynamics*. Oxford Science Publications, Oxford, 1986.

[60] A. J. Kovacs. Glass transition in amorphous polymers: a phenomenological study. *J. Polym. Sci.*, 30(3):131–147, 1958.

[61] L. C. E. Struik. *Physical Aging in Amorphous Polymers and Other Materials*. Elsevier, Oxford, 1978.

[62] R. S. Hoy and M. O. Robbins. Strain hardening in polymer glasses: Limitations of network models. *Physical Review Letters*, 99:117801, 2007.

[63] K. Chen, E.J. Saltzman, and K.S. Schweizer. Segmental dynamics in polymers: from cold melts to ageing and stressed glasses. *J. Phys. : Condens. Matter*, 21:503101, 2009.

[64] F. Ritort and P. Sollich. Glassy dynamics of kinetically constrained models. *Advances in Physics*, 52:219–342, 2003.

[65] J. P. Garrahan and D. Chandler. Geometrical explanation and scaling of dynamical heterogeneities in gass forming systems. *Phys. Rev. Lett.*, 89:035704, 2002.

[66] C. B. Roth, editor. *Polymer Glasses*. CRC Press, Boca Raton, 2016.

[67] G.A. Medvedev and J.M. Caruthers. Predictions of volume relaxation in glass forming materials using a stochastic constitutive model. *Macromolecules*, 48:788–800, 2015.

[68] D. J. A. Senden, S. Krop, J. A. W. van Dommelen, and L. E. Govaert. Rate- and temperature-dependent strain hardening of polycarbonate. *Journal of Polymer Science Part B: Polymer Physics*, 50:1680–1693, 2012.

[69] V.-D. Vogt, M. Dettenmaier, H.W. DSpiess, and M. Pietralla. Orientation of the diphenylene propane unit in stretched polycarbonate from two-dimensional magic-angle-spinning nmr. *Colloid Polym. Sci.*, 268:22–27, 1990.

[70] T. Ge and M. O. Robbins. Anisotropic plasticity and chain orientation in polymer glasses. *Journal of Polymer Science Part B: Polymer Physics*, 48:1473–1482, 2010.

[71] H.G.H Van Melick, L.E. Govaert, B. Raas, W.J. Nauta, and H.E.H. Meijer. Kinetics of ageing and re-embrittlement of mechanically rejuvenated polystyrene. *Polymer*, 44:1171–1179, 2003.

[72] C.C.W.J. Clarijs and L.E. Govaert. Strain hardening in in glassy polymers: influence of network density on elastic and viscous contributions. *J. Polym. Sci. Part B: Polym. Phys.*, 57:1001–1013, 2019.

[73] L.C.A. van Breemen, T.A.P. Engels, E.T.J. Klompen, D.J.A. Senden, and L.E. Govaert. Rate- and temperature-dependent strain softening in solid polymers. *J. Polym. Sci. Part B: Polym. Phys.*, 50:1589–1596, 2019.

[74] L. Conca. *Mechanical properties of polymer glasses : Mechanical properties of polymer glasses, chapter 3, pages 81-90*. PhD thesis, Lyon, 2016.

[75] R. S. Hoy and C. S. O'Hern. Viscoplasticity and large-scale chain relaxation in glassy-polymeric strain hardening. *Physical Review E*, 82:041803, 2010.

[76] GB McKenna. Mechanical rejuvenation in polymer glasses: fact or fallacy? *J. of Phys. Cond. Matt*, 15(11, SI):S737–S763, 2003. 3rd Workshop on Non-Equilibrium Phenomena in Supercooled Fluids, Glasses, and Amorphous Materials, PISA, ITALY, SEP 22-27, 2002.

[77] G.A. Medvedev and J.M. Caruthers. Development of a stochastic constitutive model for prediction of postyield softening in glassy polymers. *J. Rheology*, 57:949–1002, 2013.

[78] R. Masurel, P. Gelineau, F. Lequeux, S. Cantournet, and H. Montes. Dynamical heterogeneities and mechanical non-linearities: Modeling the onset of plasticity in polymer in the glass transition. *Eur. Phys. J. E*, 40:116, 2017.

[79] W.Z. Zou and R.G. Larson. A hybrid brownian dynamics/constitutive model for yielding, aging, and rejuvenation in deforming polymeric glasses. *Soft Matter*, 12: 6757–6770, 2016.

[80] W.Z. Zou, S. Moghadam, R.S. Hoy, and R.G. Larson. Multiscale modeling of sub-entanglement-scale chain stretching and strain hardening in deformed polymeric glasses. *Macromolecules*, 52:9248–9260, 2019.

[81] D.J.A. Senden, J.A.W. van Dommelen, and L.E. Govaert. Physical aging and deformation kinetics of polycarbonate. *J. Polym. Sci. Part B: Polym. Phys.*, 50:1589–1596, 2012.